



Constructing a geography of heavy-tailed flood distributions: insights from common streamflow dynamics

Hsing-Jui Wang¹, Ralf Merz^{1,2}, and Stefano Basso³

¹Department of Catchment Hydrology, Helmholtz Centre for Environmental Research – UFZ, Halle (Saale), 06120, Germany,

²Institute of Geosciences and Geography, Martin-Luther University Halle-Wittenberg, Halle (Saale), 06120, Germany,

³Department of Geography, Norwegian University of Science and Technology, Trondheim, 7491, Norway

Correspondence to: Hsing-Jui Wang (hsing-jui.wang@ufz.de)

Abstract. Heavy-tailed flood distributions depict the higher occurrence probability of extreme floods. Understanding the spatial distribution of heavy tail floods is essential for effective risk assessment. Conventional methods often encounter data limitations, leading to uncertainty across regions. To address this challenge, we utilize hydrograph recession exponents derived from common streamflow dynamics, which have shown to be a robust indicator of flood tail propensity across analyses with varying data lengths. Analyzing extensive datasets covering the Atlantic Europe, Northern Europe, and the continental United States, we uncover distinct patterns: prevalent heavy tails in the Atlantic Europe, diverse behavior in the continental United States, and predominantly nonheavy tails in Northern Europe. The regional tail behavior has been observed in relation to the interplay between terrain and meteorological characteristics, and we further conducted quantitative analyses to assess the influence of hydroclimatic conditions using Köppen classifications. Notably, temporal variations in catchment storage are a crucial mechanism driving highly nonlinear catchment responses that favor heavy-tailed floods, often intensified by concurrent dry periods and high temperatures. Furthermore, this mechanism is influenced by various flood generation processes, which can be shaped by both hydroclimatic seasonality and catchment scale. These insights deepen our understanding of the interplay between climate, geographical settings, and flood behavior, while highlighting the utility of hydrograph recession exponents in flood hazard assessment.



25 1 Introduction

Floods are devastating natural hazards that pose significant risks to infrastructure, property, and human life (McDermott, 2022; Bevere and Remondi, 2022). The unprecedented magnitude of extreme floods often characterizes these hazards, which is better depicted by the heavy-tailed behavior exhibited in flood frequency distributions (Smith et al., 2018; Merz et al., 2021; Merz et al., 2022). The concept of heavy-tailed behavior finds broad application in various fields to describe the likelihood of extreme event occurrences (Katz et al., 2002; Kondor et al., 2014; Malamud, 2004; Sartori and Schiavo, 2015; Wang et al., 2022). In particular, it is widely recognized as a prevalent feature in hydrologic extremes (Papalexioiu and Koutsoyiannis, 2013; Smith et al., 2018). While acknowledging various statistical definitions of heavy-tailed distributions (e.g., Gumbel, 1958; Hosking, 1990; Werner and Upper, 2002; El Adlouni et al., 2008; Merz et al., 2022; Nair et al., 2022), we have identified a theoretical control on the occurrence of power-law-tailed flows (Wang et al., 2023), which is one type of heavy-tailed distribution and indicates a substantial probability of extreme floods.

To organize current knowledge on the drivers and underlying mechanisms of heavy-tailed flood distributions, Merz et al. (2022) conducted an extensive review of current studies and summarized their findings into nine hypotheses. Notably, they pointed out that while one might intuitively assume that heavy-tailed flood distributions are inherited from heavy-tailed rainfall distributions, the evidence does not always support this hypothesis. For instance, a study by McCuen and Smith (2008) revealed that cases with skewed rainfall distributions, implying longer and heavier tails, do not necessarily translate into skewed flood distributions. This finding is supported by similar results from Sharma et al. (2018), who discovered that although there has been a significant increase in rainfall extremes, a corresponding increase in flood extremes is not observed. Indeed, Gaume (2006) pointed out that the asymptotic behavior of flood distributions is primarily controlled by rainfall distributions only for situations with very large return periods.

In the review of Merz et al. (2022), it becomes evident that multiple hydro-physiographic characteristics interact within a complex system, collectively shaping flood tail behavior. Specifically, the interplay between characteristic flood generation (Bernardara et al., 2008; Thorarinsdottir et al., 2018), the presence of mixed flood types (Morrison and Smith, 2002; Villarini and Smith, 2010), the tail heaviness of rainfall distributions (Gaume, 2006), catchment aridity (Molnar et al., 2006; Merz and Blöschl, 2009; Guo et al., 2014), and catchment area (Pallard et al., 2009; Villarini and Smith, 2010) are proposed as contributing factors to the nonlinearity of catchment responses. This nonlinearity is increasingly recognized as a plausible driver of heavy-tailed flood behavior (Fiorentino et al., 2007; Struthers and Sivapalan, 2007; Gioia et al., 2008; Rogger et al., 2012; Basso et al., 2015; Merz et al., 2022; Basso et al., 2023; Wang et al., 2023).

The nonlinearity of catchment hydrological responses manifests in the hydrograph recession behavior, commonly described by a power law function (Brutsaert and Nieber, 1977; Biswal and Marani, 2010; Tashie et al., 2020a):

$$\frac{dq}{dt} = -B \cdot q^a$$

Here, q represents streamflow, t denotes time, and B and a are empirical constants referred to as the recession coefficient and exponent, respectively. Particularly, the recession exponent a is used to express linear to nonlinear responses. Higher a values indicate streamflow behavior with quicker rise for a peak and faster decay during high flow, while slower decay and more stability during low flow (Tashie et al., 2019). Given that a higher recession exponent reflects significant nonlinearity in catchment responses, it has been proposed as an indicator of the emergence of heavy-tailed flood distributions (Basso et al., 2015; Wang et al., 2023).

In our prior research (Wang et al., 2023), we introduced hydrograph recession exponents as a newly proposed indicator for heavy-tailed flood behavior. This indicator allows for inference of heavy-tailed flood distributions based on physical mechanisms (i.e., typical hydrological processes within common streamflow dynamics). Importantly, it has shown its capacity to provide robust estimates for both short and long data records. This is mainly because it infers heavy-tailed behavior from common discharge dynamics, which allows for a more effective use of information contained in the data. For instance, when working with a 10-year data series, only 12 samples are available for annual



70 maxima analysis, while a much larger number of recession events (an average of 400 in Wang et al., 2023) can possibly be used for estimating hydrograph recession exponents and inferring from this the flood tail behavior.

The reliable estimation of tail heaviness is acknowledged to be challenging due to data sensitivity issues. Wietzke et al. (2020) employed bootstrap experiments to evaluate data sensitivity of four frequently used indices (i.e. shape parameter of the generalized extreme value (GEV) distribution, upper tail ratio, Gini index, and obesity index), highlighting prevalent concerns, particularly for cases with heavier tails. Studies based on goodness-of-fit tests for Generalized Extreme Value (GEV) distributions suggested that 30 to 40 samples are necessary for reliable estimation (Cai and Hames, 2010; Németh et al., 2020). Additional efforts to enhance reliability include the application of L-moments, as demonstrated by Hosking et al. (1985) for improved upper tail estimation of GEV compared to maximum likelihood, and L-moment ratio diagrams, shown by Vogel and Fennessey (1993) for enhanced estimation in highly skewed samples. Besides advancements in tail heaviness indices and parameter estimation methods, the reduced demands on data length for estimating tail behavior through the hydrograph recession exponent present an alternative solution to this issue. Particularly, the consistent estimates of flood tail heaviness across various data lengths based on hydrograph recession exponents suggest its potential value as a tool for analyzing regions with diverse gauge data records.

85 Numerical experiments conducted on data from 98 German catchments revealed that a minimum of approximately 10 years of monthly maximum data is necessary to obtain consistent estimates of the GEV shape parameter on a seasonal basis. In contrast, our proposed indicator shows consistent performance even with record lengths of 3-5 years (see Figure 3; Wang et al., 2023).

90 Our aim in this following work is to construct a geography of flood tail behavior based on the inferred heavy-tailed flood ‘hotspots’, recognized by this indicator, thus ensuring comparability of analyses across different data lengths. Given that longer and comparable record lengths are desirable for analyzing heavy-tailed distributions using conventional methods (Cunderlik and Burn, 2002; Papalexiou and Koutsoyiannis, 2013), and considering the global variation in available hydrological data lengths (Lins, 2008), this work contributes to filling the research gap by providing a reliable estimation of heavy-tailed flood behavior across a wide range of geography (Merz et al., 2022). Specifically, our objectives are twofold: (1) to validate the effectiveness of recession exponents in identifying heavy-tailed flood behavior through an extensive analysis, and (2) to investigate the underlying factors related to diverse physiographical settings, taking into account spatial patterns, seasonality, and catchment scale characteristics, and how they influence catchment nonlinearity, leading to the emergence of heavy-tailed floods.

100 We organize the structure of this paper as follows: Section 2 describes the study areas and the hydrological data based on an extensive dataset composed of four countries, Section 3 describes the methods of estimation and validation of hydrograph recession exponents in identifying heavy-tailed flood behavior in the dataset, the framework of the analyses of spatial patterns of inferred heavy-tailed flood behavior, the framework of the analyses of seasonal dynamics of inferred heavy-tailed flood behavior, and statistical tests. In Section 4, we present the validation results of our heavy-tailed flood behavior index, along with analyses of the relationships between flood tail behavior and geographical spatial characteristics, seasonal patterns, and catchment scales in these comparable countries. Physical interpretations of the results and remarks from the literature are discussed in Section 5. The main conclusions are summarized in Section 6.

2 Study areas and data

110 We conducted analyses based on datasets covering three main regions: Atlantic Europe, Northern Europe, and the continental United States. Our dataset for Atlantic Europe includes river gauges of catchments in Germany and the United Kingdom. The former exhibits a larger variation in elevation, ranging from sea level to 2,962 meters, while the latter is generally flatter, with elevations ranging from sea level to 1,345 meters. Northern Europe is characterized by strong snow dynamics in flood generation processes, setting it apart from the other regions in this study. The continental United States represents the most diverse region in terms of physiographical settings, allowing us to validate and consolidate the transferability of our findings. We aim to select catchments with low anthropogenic influences and long continuous records. Specifically, the Model Parameter Estimation Experiment dataset (MOPEX, Duan et al., 2006) is used for the continental United States, which claims an exclusion of strong effects from human activities. The Global Runoff Data Centre (GRDC, Bundesanstalt für Gewässerkunde, 2022) provided runoff data



120 with continuous records spanning more than 50 years for Norway and the United Kingdom, contributing to the dataset
for Northern Europe and part of the Atlantic Europe. Additionally, the dataset from Germany, collected by Tarasova
et al. (2018), was utilized for another part of the Atlantic Europe. For all the datasets, we excluded catchments where
flows were reported to be disturbed by large reservoirs or control gates (Lehner et al., 2011; Wang, Walter et al., 2022),
or where visual examination revealed obvious flow disturbances. A total of 575 river gauges were selected from an
125 initial pool of 797 based on these criteria. We collected daily continuous streamflow records with a median recording
length of 62 years (ranging from 24 to 148 years, covering the years 1872-2021) across these regions. The
corresponding drainage areas range from 4 to 40,504 km², with a median of 1,240 km² (refer to Table A1 for detailed
information of each region).

Our analysis was performed on a seasonal basis, considering spring (March-May), summer (June-August), autumn
(September-November), and winter (December-February) to account for the seasonality of hydrograph recessions
130 (Tashie et al., 2020b) and flood distributions (Durrans et al., 2003). Each analysis conducted on a specific river gauge
during a season was treated as a case study. Consistent with previous studies (e.g., Botter et al., 2007a; Botter et al.,
2010; Ceola et al., 2010; Doulatyari et al., 2015; Basso et al., 2021; Basso et al., 2023), we chose case studies in the
Atlantic Europe and the continental United States characterized by limited snowfall, which minimizes the potential
135 transfer of water across seasons due to strong snow accumulation and melting. Specifically, this condition is defined
as having an average daily temperature below zero degrees Celsius during precipitation events for over 50% of a
season (Basso et al., 2021). However, recognizing that recession exponents can inherently capture both linear and
nonlinear catchment responses, we intentionally included case studies in Northern Europe, which are characterized by
a dominant runoff generation process driven by snow dynamics. This deliberate inclusion provides a counter-
140 verification, allowing us to explore the capability of the recession exponent as a measure of flood tail behavior in
regions primarily characterized by snowmelt-driven flood generation processes. In summary, this analysis
encompasses regions dominated by both rainfall-driven and snowmelt-driven floods, providing an extensive
examination of these factors. These procedures resulted in a total of 1997 case studies, distributed as follows: 540 in
spring, 520 in summer, 543 in autumn, and 394 in winter (refer to Table A1 for detailed information of each region).

Köppen climate classification and the derived potential evapotranspiration are employed to describe and categorize
145 the hydroclimatic characteristics of the study regions. The Köppen climate classification is sourced from the work of
Beck et al. (2018), providing high-resolution (1-km) maps that depict present-day conditions (1980-2016).
Concurrently, the derived potential evapotranspiration is obtained from the research presented by Zomer and Trabucco
(2022), offering high-resolution (1-km) maps that illustrate monthly average data (1970-2000). The latter is based on
the Food and Agriculture Organization application of the Penman-Monteith equation (FAO-56, Allen et al. 1998; Fick
150 and Hijmans, 2017).

3 Methods

3.1 Inferring Heavy Tails of Flood Distributions from Common Streamflow Dynamics

We adopt a framework of the Physically-based Extreme Value (PHEV) distribution of river flows, introduced by
Basso et al. (2021). This framework offers a mechanistic-stochastic characterization of both the magnitude and
155 probability of flows, underpinned by essential hydrological processes like precipitation, infiltration,
evapotranspiration, soil moisture, and runoff generation within river basins, as previously described in well-
established mathematical description (Laio et al., 2001; Porporato et al., 2004; Botter et al., 2007b, 2009). Specifically,
rainfall is described as a marked Poisson process with frequency λ_p [T⁻¹] and exponentially distributed depths with
average α [L]. Soil moisture increases due to rainfall infiltration and decreases due to evapotranspiration. The latter
160 is represented by a linear function of soil moisture between the wilting point and an upper critical value expressing
the water holding capacity of the root zone. Runoff pulses occur with frequency $\lambda < \lambda_p$ when the soil moisture
exceeds the critical value. These pulses replenish a single catchment storage, which drains according to a nonlinear
storage-discharge relation. The related hydrograph recession is described via a power law function with exponent
 α [-] and coefficient K [L^{1-a}/T^{2-a}] (Brutsaert and Nieber, 1977), which allows for mimicking the joint effect of
165 different flow components (Basso et al., 2015). The description of runoff generation and streamflow dynamics
provided by this framework has been successfully tested across a diverse range of hydroclimatic and physiographic
conditions through a number of studies (Arai et al., 2020; Botter et al., 2007a; Botter et al., 2010; Ceola et al., 2010;



Doulatyari et al., 2015; Mejía et al., 2014; Müller et al., 2014; Müller et al., 2021; Pumo et al., 2014; Santos et al., 2018; Schaeffli et al., 2013).

170 Within the PHEV framework, we obtain consistent expressions for the probability distributions of various flow metrics, including daily streamflow (Botter et al., 2009), ordinary peak flows (local flow peaks resulting from streamflow-producing rainfall events), and floods (flow maxima within a specified timeframe) (Basso et al., 2016). The mathematical expressions for these are presented as Eqs. (1) to (3), respectively:

$$p(q) = C_1 \cdot q^{-a} \left(e^{\frac{-1}{\alpha K(2-a)} q^{2-a}} \right) \left(e^{\frac{\lambda}{K(1-a)} q^{1-a}} \right), \quad (1)$$

$$175 \quad p_j(q) = C_2 \cdot q^{1-a} \cdot e^{-\frac{q^{2-a}}{\alpha K(2-a)}} \cdot e^{\frac{q^{1-a}}{K(1-a)}}, \quad (2)$$

$$p_M(q) = p_j(q) \cdot \lambda \tau \cdot e^{-\lambda \tau \cdot D_j(q)}, \quad (3)$$

where $D_j(q) = \int_q^\infty p_j(q) dq$, τ [day] is the duration of the considered time frame, C_1 and C_2 are normalization constants.

180 By taking the limit of these distributions, insights into the tail behavior of these theoretical flow distributions are obtained (Basso et al., 2015; Wang et al., 2023) (see Eqs. (4) to (6), set $C_3 = \lambda \tau C_2$). Wang et al. (2023) showed that the tail of the distribution is exclusively governed by a power law function (indicating heavy tails) when the hydrograph recession exponent exceeds two, signifying discernible nonlinearity of catchment responses. Conversely, the tail appears as nonheavy when the recession exponent is below two, suggesting linearity of catchment responses (notice that recession exponents are found to be above one in most river basins; Biswal and Kumar, 2014; Tashie et al., 2020b). As a result, the hydrograph recession exponent has been proposed as a suitable indicator of heavy-tailed flood behavior, based on the analysis of common discharge dynamics. For further detailed information, please refer to Wang et al (2023).

$$\lim_{q \rightarrow +\infty} p(q) = \lim_{q \rightarrow +\infty} \left\{ C_1 \cdot q^{-a} \left(e^{\frac{-1}{\alpha K(2-a)} q^{2-a}} \right) \left(e^{\frac{\lambda}{K(1-a)} q^{1-a}} \right) \right\}, \quad (4)$$

$\begin{matrix} \mapsto 0 & \mapsto 0 & \mapsto e^0 = 1 & \text{for } 1 < a < 2 \\ \underbrace{\hspace{1.5cm}} & \underbrace{\hspace{1.5cm}} & \underbrace{\hspace{1.5cm}} & \\ \mapsto 0 & \mapsto e^0 = 1 & \mapsto e^0 = 1 & \text{for } a > 2 \end{matrix}$

$$\lim_{q \rightarrow +\infty} p_j(q) = \lim_{q \rightarrow +\infty} \left\{ C_2 \cdot q^{1-a} \left(e^{\frac{-1}{\alpha K(2-a)} q^{2-a}} \right) \right\}, \quad (5)$$

$\begin{matrix} \mapsto 0 & \mapsto 0 & \text{for } 1 < a < 2 \\ \underbrace{\hspace{1.5cm}} & \underbrace{\hspace{1.5cm}} & \\ \mapsto 0 & \mapsto e^0 = 1 & \text{for } a > 2 \end{matrix}$

$$190 \quad \lim_{q \rightarrow +\infty} p_M(q) = \lim_{q \rightarrow +\infty} \left\{ C_3 \cdot q^{1-a} \left(e^{\frac{-1}{\alpha K(2-a)} q^{2-a}} \right) \right\}, \quad (6)$$

$\begin{matrix} \mapsto 0 & \mapsto 0 & \text{for } 1 < a < 2 \\ \underbrace{\hspace{1.5cm}} & \underbrace{\hspace{1.5cm}} & \\ \mapsto 0 & \mapsto e^0 = 1 & \text{for } a > 2 \end{matrix}$

We employ an event-based analysis for estimating hydrograph recession exponents, a method deemed more robust than cloud-based analysis (Biswal and Marani, 2010; Dralle et al., 2017; Jachens et al., 2020). Specifically, we estimate the parameters of empirical power laws for individual hydrograph recessions through a linear regression of the pairs of dq/dt and q in log-log scale. The constant time step (CTS) method has been commonly used in various studies to estimate the time derivatives dq/dt (e.g., Biswal and Marani, 2010; Mutzner et al., 2013; Dralle et al.,



200 2017; Tashie et al., 2020b; Basso et al., 2023), while other methodologies (Wittenberg, 1999; Rupp and Selker, 2006;
Roques et al., 2017) have been developed for specific conditions. For instance, the exponential time step (ETS) method
was introduced to reduce estimation uncertainty mainly caused by the latter-stage (low-flow) recession (Roques et al.,
2017). In this study, recession exponents have been calculated using both CTS and ETS methods, yielding similar
conclusions regarding flood tail behavior (see supporting information Text S1 and Figure S1). Therefore, we chose to
base the subsequent analyses on the results obtained from the more commonly utilized approach (i.e., the CTS). The
supporting information, Figure S2, provides an example of this process. The initiation of a recession event is defined
as an ordinary peak of daily discharge that surpasses the mean discharge over the entire discharge records (Biswal and
Marani, 2010; Mutzner et al., 2013). We incorporate the entire recession process in the estimation of power law
exponents (which has been shown as crucial in shaping flood frequency behavior; Guo et al., 2014; Basso et al., 2016),
meaning both the peak and the subsequent daily streamflow decay are included without excluding any days (Dralle et
al., 2017). This decision ensures that we account for the effects of both fast, mainly associated with surface (early
stage of recession) and slow, mainly associated with subsurface flows (late stage of recession) on catchment nonlinear
responses in the adopted recession analysis (Barnes, 1939; Chen and Krajewski, 2016; Mathai and Mujumdar, 2022).
210 This procedure marks the pivotal difference between the adopted analysis and those solely focused on the recession
behavior of low flow/baseflow (Figure S3 in the supporting information provides a schematic diagram of hydrograph
recession analysis adopted in this study). The minimum duration of a recession is set to five days (Dralle et al., 2017),
denoting that recessions shorter than five days are not considered. Finally, we determine the median value of estimated
exponents across all identified events as the representative value to ensure robustness (Dralle et al., 2017; Jachens et
al., 2020).
215

3.2 Validation of Hydrograph Recession Exponents as An Index of Heavy-Tailed Flood Behavior

To validate the identification of heavy-tailed flood behavior obtained through estimated recession exponents, we fit a
power law distribution to the empirical data distribution and evaluate the reliability of empirical power laws, serving
as the benchmark of heavy-tailed flood behavior presented by data.

220 A case study is considered to exhibit heavy-tailed behavior if the empirical power law effectively describes the tail
behavior of the data distribution. We used the Kolmogorov-Smirnov (KS) statistic (κ) to preliminarily assess empirical
power law distribution reliability ($\kappa \in [0, \infty]$, with $\kappa=0$ denoting highest reliability) (Clauset et al., 2009; Klaus et al.,
2011; Alstott et al., 2014). We acknowledge that there are alternative methods for evaluating goodness-of-fit. For
example, the Anderson-Darling test, which is essentially a modified version of the Kolmogorov-Smirnov test, gives
225 greater weight to the tails when assessing the distance between distributions. However, using such tests can be more
conservative in determining the minimum threshold of the variable that delineates the tail range of the empirical
distribution. This characteristic necessitates a much larger dataset to ensure a robust distribution fit for the tail;
otherwise, the sample size of the identified tail may be insufficient for a reliable fit (Alstott et al., 2014; Clauset et al.,
2009). In our case, we opted for the KS test because it allows for more appropriate sample sizes based on our datasets
230 (Hosking and Wallis, 1987) (see Figure S4 in the supporting information). To establish the reference point for plausible
empirical power laws, we employed the framework introduced by Clauset et al. (2009). The upper tail of the discharge
distribution is fitted with empirical power laws using the method of maximum likelihood. The upper tail is defined by
an optimized lower boundary of the discharge, determined by selecting the best fit based on the KS statistic. The
goodness-of-fit test is conducted using the KS test with a significance level of $p > 0.1$. It's important to note that a
235 higher p -value is considered more rigorous in this context, as the aim is to verify the null hypothesis rather than to
reject it, as is often considered in other cases. Thus, $p > 0.1$ is a more stringent criterion than $p > 0.05$ in this scenario.
All cases that meet the goodness-of-fit criteria are further evaluated for plausibility against common alternative
distributions using the bootstrapping method. This involves generating 1000 sets of synthetic data from the optimized
power law model, each with the same sample size as the fitted observations. In their experiments, the number of 1000
240 repetitions has proven sufficient to distinguish power laws from both exponential and lognormal distributions using
the KS test with a $p > 0.1$ significance level. Once the empirical power law passes all these criteria, it is considered a
dependable (plausible) representation of the empirical data distribution. We term such a case study a 'power-law-tailed
case study,' while cases that don't meet these criteria are labeled as 'uncertain case studies' in subsequent analyses. The
latter label acknowledges the awareness that we cannot definitively conclude whether these case studies are indeed
245 not power-law-tailed or if their underlying distributions cannot be determined due to the high uncertainty caused by
the small sample sizes of available observations. We conduct these computations using the Python package `pfit` 1.0.3.



We calculate empirical power law exponents b for each case and assess the consistency of identifying heavy-tailed behavior using both a and b .

250 We conduct our approach using three distinct empirical data distributions: daily streamflow, ordinary peaks, and monthly maxima. The sample sizes of the identified upper tails for the distributions of daily streamflow range from 176 to 11260, with a median of 1280. For the distributions of ordinary peaks, the sample sizes range from 13 to 2240, with a median of 512. In the case of monthly maxima distributions, the sample sizes vary from 6 to 418, with a median of 132. These multiple analyses strengthen our validation process and enhance the evaluation of our results. It's worth
255 noting that our chosen benchmark, the empirical power law, may be influenced by fitting uncertainty due to data scarcity in certain cases, particularly when analyzing maxima. To mitigate this, we consider monthly maxima (Fischer and Schumann, 2016; Malamud and Turcotte, 2006) instead of the seasonal maxima previously used in the literature (e.g., Basso et al., 2021) in order to expand the sample size. Parallel analyses for cases with larger sample sizes (i.e., daily streamflow and ordinary peaks) provide more robust validation and lend support to the interpretation of results for maxima. We acknowledge that the method of maximum likelihood used for parameter estimation could, in
260 principle, be substituted with various established approaches based on the characteristics of the study data. For instance, Hosking and Wallis (1987) shown that the method of probability-weighted moments could offer better parameter estimation when working on less than 500 samples for generalized Pareto distributions, which are known to exhibit power law tails in asymptotic analysis.

3.3 Analyses of Spatial and Seasonal Patterns of Inferred Flood Tail Behavior

265 We construct a geographical representation of inferred heavy-tailed flood behavior by utilizing estimated recession exponents derived from common streamflow dynamics across study countries and for each season. This representation serves as an evaluation of the propensity of heavy-tailed flood behavior across various regions and seasons. We simplify the seasonal results by identifying the dominant tail behavior, which refers to the majority of seasons exhibiting either heavy-tailed or nonheavy-tailed behavior, as the representative inferred flood tail behavior in the
270 analysis of spatial pattern (Section 4.2).

To determine the dominant hydroclimatic characteristic of each catchment, we overlay the Köppen climate map (Beck et al., 2018) and a derived potential evapotranspiration map (Zomer and Trabucco, 2022) with the river gauge and catchment boundary data. For the former, the most prevalent climate within the catchment (determined by overlapping areas within the boundary, or by the river gauge location if the boundary data is absent) is assigned as the representative
275 feature. For the latter, we compute the catchment average value (or determined by the river gauge location if the boundary data is absent).

To analyze seasonal patterns, we initially investigate the coherence of inferred flood tail behavior across seasons, focusing on consistency between heavy- or nonheavy-tailed behavior. Catchments with valid recession exponents from only one season are omitted from this analysis. As a result, the selection comprises 179 out of 180 catchments
280 in the Atlantic Europe, 79 out of 82 in Northern Europe, and 290 out of 313 in the continental United States. We also employ the Wilcoxon signed-rank test (Wilcoxon, 1945), a non-parametric statistical hypothesis test, at a significance level of 0.05 in this section. This test assesses whether the median of recession exponents (within a climate group on a seasonal basis) is above two, below two, or shows no significant difference from two (Figure 7).

4 Results

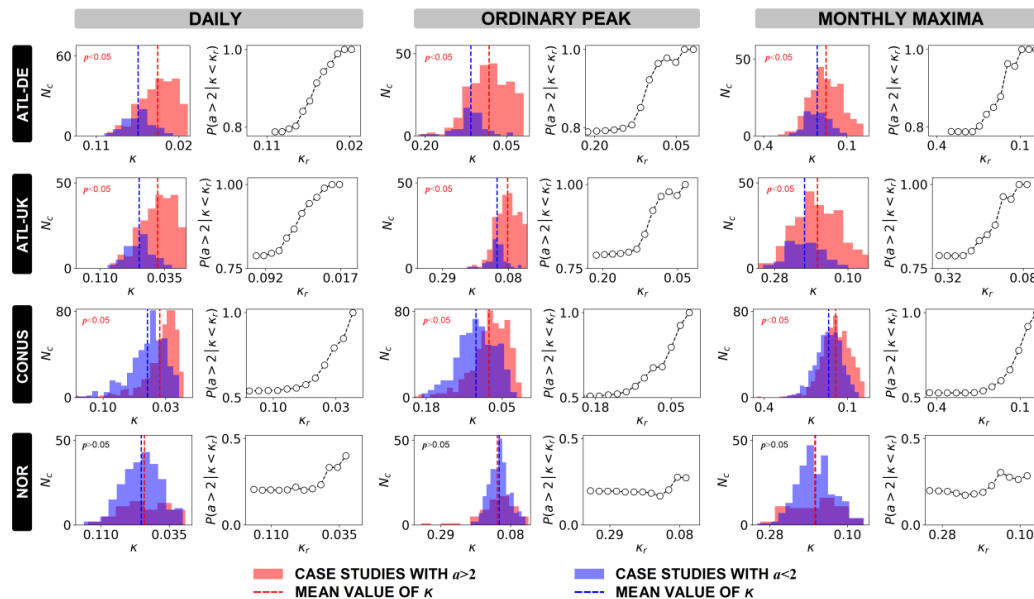
285 4.1 Effectiveness of Identifying Heavy-tailed Flood Behavior Using Common Discharge Dynamics

Figure 1 shows the frequency histograms of KS statistics κ for two groups of cases: red histograms denote cases with recession exponents a above two, and blue histograms denote those below two. The mean κ is significantly smaller ($p < 0.05$) for the former group (red histograms) compared to the latter one (blue histograms) for the case studies from the Atlantic Europe (both Germany and the UK) and the continental United States. This result shows that power law
290 distributions (characterized by heavy-tailed behavior) better represents the empirical data in case studies with recession exponents above two. In the Norwegian case studies, no significant difference was instead identified between the two groups. This is likely due to the absolute values of the recession exponent in this context, which is lower than



in the other three countries and mostly comprised between 1 and 2, thus indicating a prevalence of nonheavy-tailed behaviors to date.

295 To quantify the accuracy provided by the identification of heavy-tailed flood behavior through recession exponents, we set decreasing thresholds for κ , which correspond to increasing reliability of power laws as descriptions of the empirical data. The accuracy of our index (i.e., the recession exponent) can therefore be calculated as $P(a > 2 | \kappa < \kappa_r) = N_c(a > 2 | \kappa < \kappa_r) / N_c(\kappa < \kappa_r)$, where κ_r is the threshold, $N_c(\kappa < \kappa_r)$ is the number of case studies with $\kappa < \kappa_r$, and $N_c(a > 2 | \kappa < \kappa_r)$ is the number of case studies with $a > 2$ among the $N_c(\kappa < \kappa_r)$ case studies. We found that the accuracy is clearly correlated to the reliability level requested for the empirical power laws (represented by κ_r) for case studies in the Atlantic Europe and the continental United States. This confirms that the recession exponent provides higher accuracy in detecting heavy-tailed behaviors when the empirical distributions of observed data can be represented by power laws with more certainty, thus underscoring the consistency between identifying heavy-tailed cases by using the proposed index and the observations. The accuracy increases in the same way also for case studies in Norway, but it always remains below 0.5. We will elucidate below reasons and implications of this finding after considering the results presented in Figure 2.



310 **Figure 1. Effectiveness of identifying heavy-tailed flood behavior using hydrograph recession exponents.** Case studies are categorized into two groups in each study region: the Atlantic Europe-Germany (ATL-DE), the Atlantic Europe-the United Kingdom (ATL-UK), Northern Europe (NOR), and the continental United States (CONUS). The group with recession exponents a above two is represented by red histograms and the group with recession exponents a below two is represented by blue histograms. In all three analyses (daily streamflow, ordinary peak flow, and monthly maxima), every case study is subjected to empirical power law fitting, resulting in a representative power law for the dataset, measured by the KS statistic κ (where $\kappa \in [0, \infty]$ and $\kappa=0$ signifies maximum reliability). The histograms portray the count of case studies N_c analyzed as a function of κ for two distinct groups. 315 Dashed lines on the histogram plots indicate the means of the histograms. The means of two groups ($a > 2$ and $a < 2$) are subjected to Welch's t-test at a significance level of 0.05 to determine whether they are significantly different ($p < 0.05$) or not ($p > 0.05$). The line chart shows the accuracy of using the recession exponent to identify heavy-tailed behavior (denoted as $P(a > 2 | \kappa < \kappa_r) = N_c(a > 2 | \kappa < \kappa_r) / N_c(\kappa < \kappa_r)$) as the κ_r threshold decreases (i.e., as the reliability of empirical power laws increases). The results for ATL-DE are reproduced from Wang et al. (2023).

320 In Figure 2, we explore the correlation between the values of empirical power law exponents b and the values of recession exponents a for case studies exhibiting heavy-tailed behavior. This is achieved by utilizing the goodness-



of-fit testing procedure of Clauset et al. (2009) to categorize case studies into ‘power-law-tailed case studies’ and ‘uncertain case studies.’ The former are depicted as black dots, while the latter are depicted as gray dots. The presence of a sizable number of uncertain case studies indicates the difficulty of establishing with certainty whether the underlying distribution of empirical data is or not a power law. This difficulty is often due to limited data availability, although the possibility that they indeed do not follow power laws cannot be excluded. We also perform an L-moment analysis, a compelling method in order statistics used to quantitatively describe extremes and known for its robustness to stochastic sampling uncertainties (Hosking, 1990). This analysis serves to confirm the tail heaviness observed in the identified power-law-tailed case studies, in which these case studies show clearly heavier tails than exponential distributions (i.e., the widely accepted distinction of heavy- and nonheavy-tailed distributions; Merz et al., 2022) (see supporting information Figure S5).

For all power-law-tailed case studies, we calculated Spearman correlations r_s (Spearman, 1904) to test the correlation between a and b , which is valid for both linear and nonlinear associations between random variables. We found that a and b are significantly correlated at a significance level of 0.05 in the Atlantic Europe (both Germany and the UK) and the continental United States. To highlight the correlation, we binned the power-law-tailed case studies and used red markers showing the median values of a and b (squares), the interquartile intervals of b (vertical bars), and the binning ranges of a . In each region, the composition of each bin encompasses one-seventh of the total number of case studies, except for Northern Europe, where this fraction is adjusted to one-fifth due to the limited number of power-law-tailed cases. In the Atlantic Europe and the continental United States, a larger number of uncertain case studies emerge in the analysis of flow maxima compared to the analysis of daily streamflow and ordinary peak flow (respectively for daily streamflow, ordinary peaks, and flow maxima: 265, 270, and 352 out of 386 case studies in Germany; 258, 280, and 306 out of 325 case studies in the UK; and 589, 624, and 836 out of 980 case studies in the continental United States). Since the same case studies have already exhibited power-law-tailed distributions in their daily streamflow and ordinary peak flow data, the increase of uncertain case studies in the analysis of flow maxima suggests that the greater level of uncertainty is due to limited data availability rather than indicating a rise in the number of non-power-law-tailed case studies.

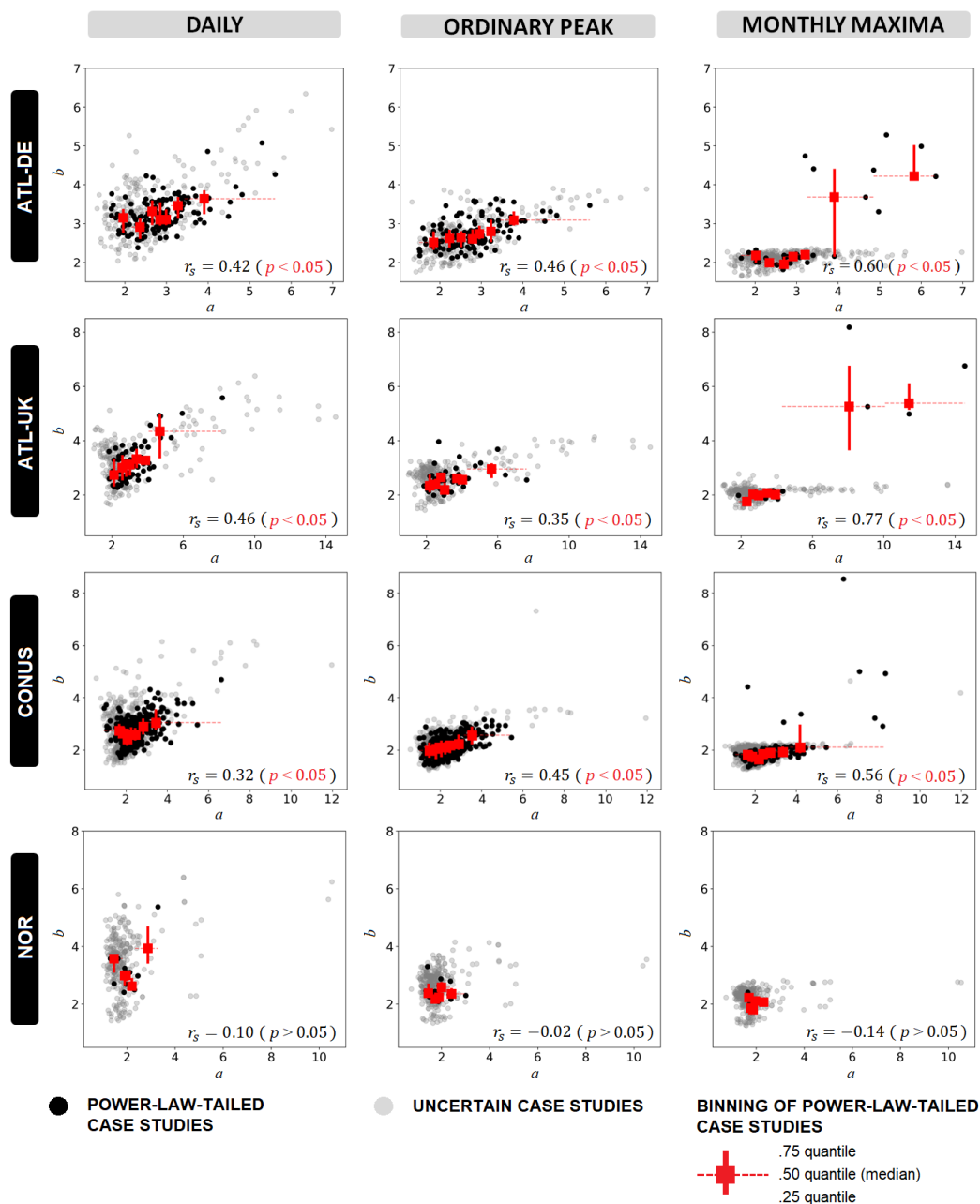
This aligns with existing literature that emphasizes the prevalence of heavy-tailed behavior when sufficiently long data records are available (e.g., Farquharson et al., 1992; Bernardara et al., 2008; Villarini and Smith, 2010; Rogger et al., 2012; Papalexiou and Koutsoyiannis, 2013; Guo et al., 2014; Basso et al., 2016; Smith et al., 2018). Such findings, on the one hand, highlight the limitations of relying solely on statistical data analyses to identify flood tail behavior. On the other hand, they underscore additional advantages of using the mechanistic approach proposed in this study, namely the hydrograph recession exponent. The utilization of the hydrograph recession exponent effectively identifies cases exhibiting heavy-tailed behavior; even in situations where statistical methods fail to confirm the underlying distribution (as observed in monthly maxima), this index still yields robust estimates of tail heaviness based on recession exponent values.

In Norway, however, the majority of case studies across all three analyses (i.e., daily streamflow, ordinary peaks, and flow maxima) are identified as uncertain (respectively 291, 289, and 300 out of 306 case studies). These results align with the fact that the values of the recession exponent for the Norwegian case studies predominantly fall between 1 and 2 (Figure 2), indicating that to date catchment responses are relatively closer to being linear in Norway compared to the other countries, and implying the prevalence of nonheavy-tailed flood behavior. This also explains the pattern presented in the Norway panel of Figure 1. Given that the case studies generally have recession exponents below two, the number of case studies with recession exponents above two are not enough to distinguish between the two distributions of κ .

Overall, the effectiveness of recession exponents in distinguishing heavy- and nonheavy-tailed flood behavior has been substantiated (see also Wang et al., 2023). This differentiation hinges on a critical threshold: the value two. In datasets showcasing diverse physiographical characteristics, the interpretation is consistent. Areas with higher recession exponents (above two), indicating discernible nonlinearity in catchment responses, tend to exhibit heavy-



tailed flood behavior. Conversely, regions with lower recession exponents (below two), reflecting relatively linear responses in catchments, are more likely to signify nonheavy-tailed flood behavior.



370

Figure 2. Empirical power law exponent b as a function of the hydrograph recession exponent a (physically-based index of heavy-tailed flood behavior). Case studies are classified into groups of power-law-tailed (black dots) and uncertain (gray dots) case studies on the basis of the goodness-of-fit test (Clauset et al., 2009). The former group shows statistical confirmation that the



375 data's distribution tail can be properly characterized by a power law, indicating heavy-tailed behavior. Conversely, the latter group
indicates our inability to statistically affirm whether the data follows a power law distribution or not. For the power-law-tailed case
studies, the correlation between the empirical power law exponent b and the hydrograph recession exponent a is underlined by red
380 markers. This correlation is quantified using the Spearman correlation coefficient r_s at a significance level of 0.05. The squares
represent the median values of a and b , vertical bars indicate the interquartile intervals of b , and horizontal dashed bars indicate the
binning ranges of a . In each region, the composition of each bin encompasses one-seventh of the total number of case studies,
except for NOR, where this fraction is adjusted to one-fifth due to the constraint posed by the total number of power-law-tailed
385 case studies. The count of the power-law-tailed case studies in the analyses of daily streamflows, ordinary peak flows, and monthly
flow maxima are as follows: 121, 116, and 34 out of 386 case studies for ATL-DE, respectively; 67, 45, and 19 out of 325 case
studies for ATL-UK, respectively; 391, 356, and 144 out of 980 case studies for CONUS, respectively; and 15, 17, and 6 out of
306 case studies for NOR, respectively. The results for ATL-DE are reproduced from Wang et al. (2023).

385 4.2 Spatial Patterns of Inferred Flood Tail Behavior

Figure 3 displays the spatial distribution of dominant flood tail behavior across seasons, based on the recession
exponent values. This dominant behavior represents either heavy or nonheavy tails, depending on what is observed in
the majority of seasons. Additionally, Figure 4 and Table 1 provide quantitative analyses of the propensity of flood
tail behavior across different regions.

390 In the Atlantic Europe-Germany (Figure 3a), approximately 81% of catchments are identified as sites with dominant
heavy-tailed flood behavior (red dots), indicating a prevalence of such behavior. This result agrees with the findings
of Mushtaq et al. (2022), which reported that a distribution with a relatively heavier tail (i.e., the log-normal) best
represent ordinary peak flows in the majority of German basins considered in their study. The inferred heavy-tailed
sites are spread across Germany. They dominate in the eastern part, while there are mixed patterns of heavy- and
395 nonheavy-tailed behavior in the western part. The climate conditions are primarily humid continental (Dfb) and
temperate oceanic (Cfb). Humid continental climate is prominent in the east, while temperate oceanic climate
generally covers the west.

In the Atlantic Europe-the UK (Figure 3b), four climate types are present, with temperate oceanic climate (Cfb) being
the dominant one. The terrain of this country in comparison to the other three countries is relatively homogeneous,
400 with no high mountains. According to our findings, heavy-tailed flood behavior is prevalent in the UK, with a
prevalence of 77%, especially in the eastern and southern coastal regions. Huntingford et al. (2014) reported a case in
which a rapid succession of vigorous Atlantic low-pressure systems crossed much of the UK, resulting in repeated
heavy rainfall events. Southeast England was identified as a distinct region characterized by exceptionally high flows,
exacerbated by increasingly saturated catchments. These catchment characteristics and hydrological responses align
405 with our findings, which indicate the pronounced heavy tails in such a region.

In Northern Europe (Norway) (Figure 3c), however, nonheavy-tailed flood behavior dominates. Approximately 89%
of sites are inferred to have nonheavy-tailed flood behavior. Norway encompasses nine climate types but is primarily
covered by Subarctic climate (Dfc), characterized by low temperatures and reduced evapotranspiration. Hydrological
processes are significantly influenced by snow dynamics, which generally determine linear catchment responses as a
410 result of snow accumulation and melting processes (Santos et al., 2018).

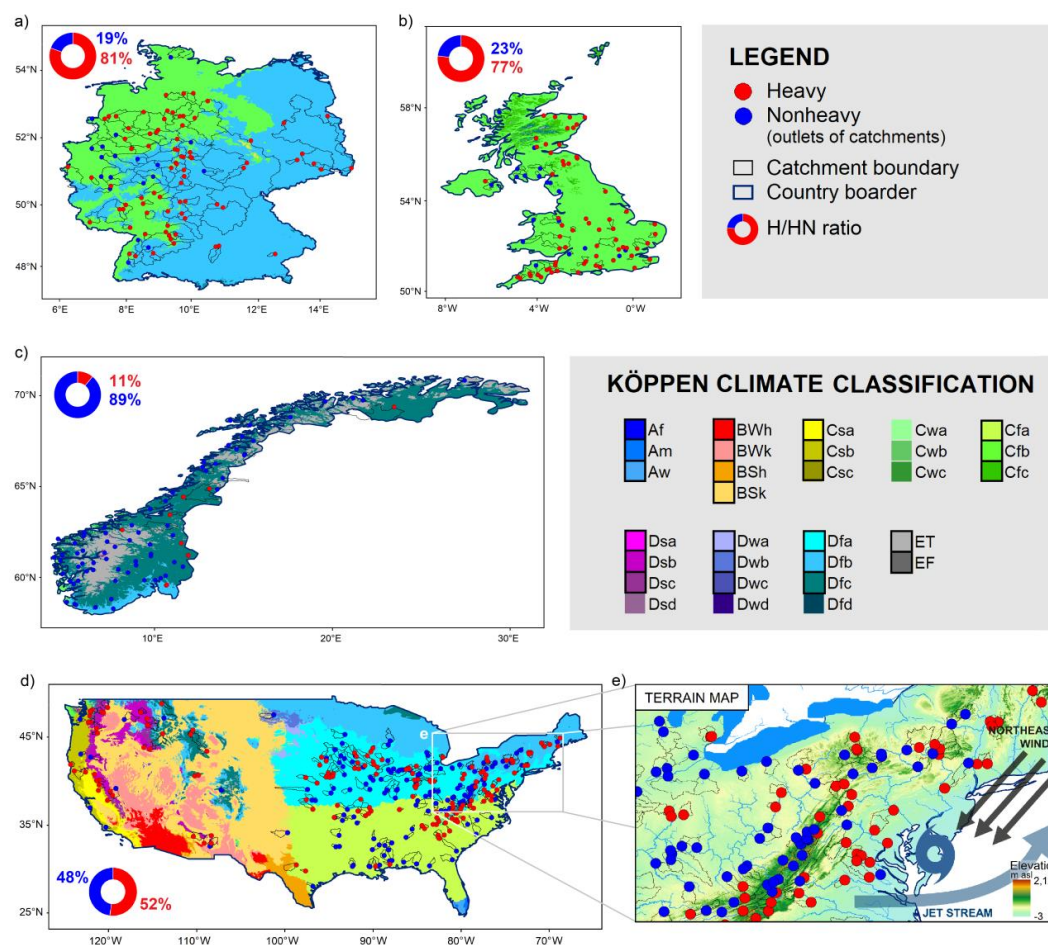
In contrast to the aforementioned countries with relatively consistent climate and dominant flood behavior, the
continental United States (Figure 3d) displays a diverse range of climate types and a balanced propensity toward
heavy- and nonheavy-tailed flood behavior. The eastern regions are dominated by humid subtropical climate (Cfa),
hot-summer humid continental climate (Dfa), and temperate oceanic climate (Cfb) from south to north. The interior
415 western states feature a cold semi-arid climate (BSk), while mixed patterns are observed in the western mountainous
and coastal areas. An overall relatively even distribution of inferred heavy-tailed (52%) and nonheavy-tailed (48%)
flood behavior prevails in this diverse climate country.

Figure 3e provides an example of how the spatial distribution of flood behavior is influenced by regional
physioclimatic features. In particular, catchments on the east side of the mountains exhibit pronounced heavy-tailed
420 flood behavior, which aligns with the findings of Smith et al. (2018). This is likely due to the interaction between cold
air from the inland polar jet stream and warm ocean currents leads to the formation of Nor'easters, which are synoptic-
scale extratropical cyclones in the western North Atlantic Ocean along the northeast coast of the continental United



States. These weather systems often resulted in heavy rain or rain-on-snow events. Conversely, on the west side of mountains, catchments tend to exhibit nonheavy-tailed behavior, potentially due to the leeward rain shadow effect.

425 In summary, the spatial distributions of inferred flood tail behavior indicate that regions with dominant climate types tend to exhibit a single or dominant flood tail behavior, as observed in the Atlantic Europe and Northern Europe areas studied in this research. Conversely, the interplay among regional physioclimatic conditions shows its impacts on the propensity of regional flood behavior across diverse climate conditions in the continental United States.



430 **Figure 3. Spatial distribution of dominant flood behavior.** The dominant pattern determines the representative flood tail behavior
 of catchments across all study countries, whether it is heavy or non-heavy, which is defined by the major pattern recognized across
 seasons. Tail behavior is inferred by hydrograph recession exponents. The ratio of heavy- to nonheavy-tailed catchments is
 indicated as H/NH ratio. Köppen climate classification based on Beck et al. (2018), with present climate types outlined by bold
 dark frames in the legend. (a) ATL-DE, a total of 98 gauges represent catchments ranging from 110 to 23,843 km², with a median
 435 area of 1,195 km². (b) ATL-UK, a total of 82 gauges represent catchments ranging from 15 to 9,948 km², with a median area of
 283 km². (c) NOR, a total of 82 gauges represent catchments ranging from 4 to 40,504 km², with a median area of 234 km². (Note:
 some catchment boundaries are absent in the dataset for catchments in the UK and Norway.) (d) CONUS, a total of 313 gauges
 represent catchments ranging from 66 to 9,935 km², with a median area of 1769 km². (e) A zoomed-in map illustrates the discernible



440 patterns of flood tail behavior resulting from specific flood generation processes influenced by the interplay between regional terrain and meteorological features. (Note: the cylinder map projection is employed in these maps.)

To obtain quantitative results we examine the predominant flood tail behavior (inferred by recession exponents) of catchments across various climate regions and sort these regions based on the proportion of heavy-tailed catchments from high to low, as illustrated in Figure 4. By categorizing climate type regions based on the proportion of heavy-tailed catchments, we establish three groups according to their propensity of flood tail behavior: Heavy-tailed group, 445 indicating regions with over 66.6% of catchments dominated by heavy tails; Neutral group, encompassing regions with 33.3% to 66.6% of catchments dominated by heavy tails, represents a relatively even propensity for both heavy and nonheavy tails in the catchments within these regions; and Nonheavy-tailed group, representing regions with less than 33.3% of catchments dominated by heavy tails, denotes the propensity for nonheavy tails. According to the Köppen climate type classification, the overarching hydroclimatic characteristics can be delineated by three 450 hierarchical features: 1. the main group, which encompasses five areas—Tropical, Arid, Temperate, Continental, and Polar; 2. precipitation characteristics; and 3. temperature characteristics (The detailed quantitative criterion adopted is provided in Table S1 in the supporting information). The findings are synthesized in Figure 4 and Table 1, where the groups of flood tail behavior propensity are juxtaposed with the distinctive traits of each climate region.

Five climate regions are identified as having a higher propensity for heavy tails: mediterranean climate (Csa), hot 455 semi-arid climates (BSH), humid continental climate (Dsb), temperate oceanic climate (Cfb), and cool-summer mediterranean climate (Csb). These regions are characterized by warm to hot temperatures, often accompanied by occasional dry periods (except for Cfb). Based on the definition of Köppen climate classification the occurrence of dry periods is a result of significantly uneven rainfall throughout the year, with at least three times as much rainfall in the wettest month as in the driest month. In semi-arid climates (BSH), there is generally lower annual rainfall 460 (summarized in Table 1). Higher temperatures increase the potential evapotranspiration, often enhancing atmospheric moisture content and facilitating convective rainfall. Moreover, the dynamics of evapotranspiration in hillslopes influence the nonlinearity of runoff processes in catchments (Tashie et al., 2019). Dry periods can lead to lower catchment soil moisture, facilitating nonlinear runoff generation (Merz and Blöschl, 2009; Viglione et al., 2009). The findings presented here indicate that heavy-tailed flood behavior tends to emerge due to the substantial nonlinearity 465 observed in catchment hydrological processes, which is facilitated by temporally uneven rainfall and higher evapotranspiration variation throughout the year.

We also find that certain regions show a relatively neutral propensity regarding flood tail behavior (either heavy- or nonheavy-tailed) and aggregate them into the second group of Figure 4 and Table 1. These regions encompass cold 470 semi-arid climates (BSk), humid continental climate (Dfb), humid subtropical climate (Cfa), and humid continental climate (Dfa). While cold semi-arid climates (BSk) experience dryness, they are characterized by very limited precipitation. In the other three regions (Dfb, Cfa, and Dfa), heavy tails may still occur due to higher evapotranspiration, which is driven by high temperatures. However, the relatively even distribution of rainfall throughout the year in these regions may reduce the propensity for heavy tails, resulting in a smoother occurrence of heavy-tailed flood behavior. In summary, the regions in this group still have a certain probability of exhibiting heavy-tailed flood behavior. However, the absence of either a drier state of the catchment (caused by uneven rainfall) or 475 higher temperatures (that ensure sufficient atmospheric moisture for rainfall and strengthened nonlinearity) could constrain the occurrence of such behavior.

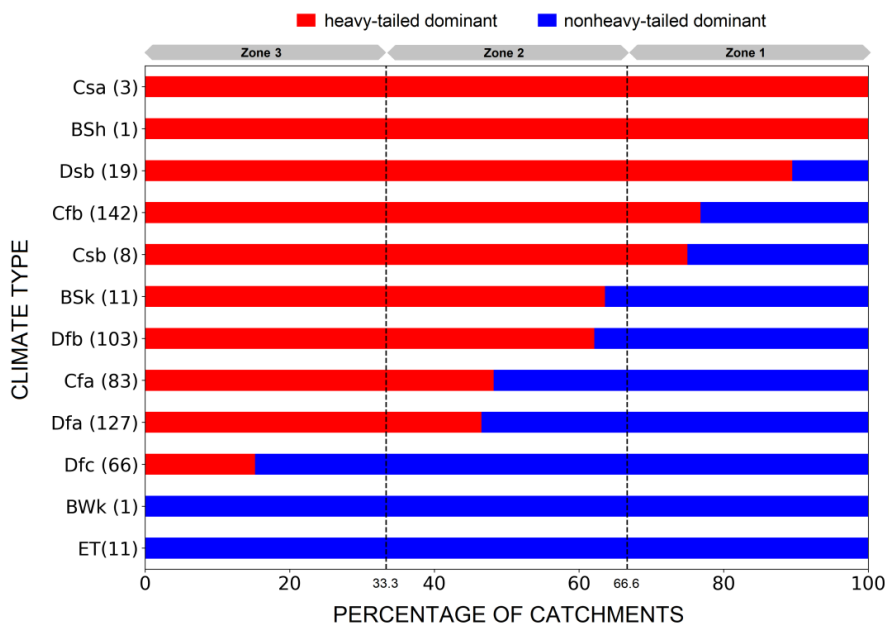
In the last group, which includes regions with subpolar climate (Dfc), tundra climate (ET), and cold desert climates (BWk), there is a higher propensity for nonheavy tails, and the two evident factors for heavy tails recognized from 480 previous results are generally lacking. Runoff generation in Dfc and ET is primarily driven by snow dynamics, with snowmelt being the main contributor to runoff. Snowmelt is highly dependent on energy capacity, resulting in hydrological responses that are more likely to exhibit linearity. This favors the occurrence of nonheavy-tailed flood behavior (Thorarinsdottir et al., 2018). Catchments located in the region of BWk exhibit nonheavy-tailed behavior might also be attributed to limited precipitation in desert.

485 In this study, we do not find substantial influences of the general hierarchical feature (especially the temperate and continental climate classifications) on the propensity of flood tail behavior.

To sum up this section, we have identified the conjunction of dry periods and higher temperatures as crucial meteorological factors significantly contributing to the dynamics of catchment storage, thereby influencing the



490 nonlinearity of hydrological responses. These findings shed light on the interplay between catchments and meteorological conditions in the manifestation of heavy-tailed flood behavior. We acknowledge that these results are based on overarching conditions and do not encompass all climate types, and achieving an equal number of study sites across various climate regions might not always be feasible. Expanding the number of study sites could further enhance our understanding, especially for extreme cases.



495 **Figure 4. Propensity of inferred flood tail behavior in diverse climate regions.** Catchments are categorized by climate types and grouped by dominant (across seasons) heavy-tailed case percentages. Three groups are defined by heavy-tailed case proportions:



Zone 1 (>66.6%) represents heavy tails, Zone 2 (33.3-66.6%) is neutral, and Zone 3 (<33.3%) represents nonheavy tails. The number of catchments in each climate region is indicated in parentheses after the climate type.

Table 1. Comparison of inferred flood tail behavior propensity with climate characteristics.

Propensity of Tail Behavior	Köppen Climate Classification					
	Code	1 st Main Group	2 nd Seasonal Precipitation	3 rd Temperature	Dry Period	Warm-Hot
Heavy (Zone 1)	Csa	Temperate	Dry Summer	Hot Summer	•	•
	BSh	Arid	Semi-Arid	Hot	•	•
	Dsb	Continental	Dry Summer	Warm Summer	•	•
	Cfb	Temperate	No dry season	Warm Summer		•
	Csb	Temperate	Dry Summer	Warm Summer	•	•
Neutral (Zone 2)	BSk	Arid	Semi-Arid	Cold	•	
	Dfb	Continental	No dry season	Warm Summer		•
	Cfa	Temperate	No dry season	Hot Summer		•
	Dfa	Continental	No dry season	Hot Summer		•
Nonheavy (Zone 3)	Dfc	Continental	No dry season	Cold Summer		
	BWk	Arid	Dessert	Cold	•	
	ET	Polar	--	Tundra		

500 4.3 Seasonal Patterns of Inferred Flood Tail Behavior

We analyze the seasonality of flood tail behavior, an aspect of this phenomenon which has been previously suggested but remains poorly understood (Durrans et al., 2003; Basso et al., 2015; Macdonald et al., 2022). Figure 5 illustrates the spatial distribution of catchments with consistent tail behavior across seasons (i.e., with either heavy or nonheavy tails across all seasons; black triangles) and those with varying tail behavior across seasons (green dots). The percentages of catchments exhibiting inconsistent flood tail behaviors are respectively 33%, 33%, 17%, and 34% in the continental United States, the Atlantic Europe-Germany, the Atlantic Europe-the UK, and Northern Europe. The results indicate that although the majority of catchments tend to exhibit stable heavy-/nonheavy-tailed behavior, still around one-third reveal changing patterns across seasons. Notably, there is a particularly high percentage of consistent patterns (83%) in the Atlantic Europe-the UK, likely due to the relatively uniform climate and terrain conditions across the country characterized by continuous rainfall throughout a year (as shown in Figure 3b).

We further investigate the dynamics of heavy- and nonheavy-tailed case studies across seasons in Figure 6. Heavy-tailed case studies increase from spring to autumn (approximately corresponding to the growing season in the northern hemisphere) and decrease from autumn to spring (approximately corresponding to the dormant season in the northern hemisphere), as seen in the aggregated patterns across all regions (panel a). This pattern can be attributed to the increasing temperature in the growing season, during which increasing evapotranspiration consumes water storage in the shallow subsurface, escalating the nonlinearity of catchment responses (Tashie et al., 2019). The seasonality of evapotranspiration effects on catchment nonlinearity is supported by the findings of Tarasova et al. (2018), who observed clear seasonal dynamics of catchment average runoff coefficients. These coefficients tend to be higher in wet winters and lower in dry summers. It has been shown that significant variation in runoff coefficients is linked to high nonlinearity of hydrological responses, facilitating heavier-tailed floods. This phenomenon is often observed in dry catchments (Merz and Blöschl, 2009). Other studies confirmed that the nonlinearity of catchment responses favors the emergence of heavy-tailed flood behavior (Gioia et al., 2008; Rogger et al., 2012; Basso et al. 2015), and is often expressed by quicker recession during high flow periods and greater stability during low flow periods. Conversely, during the dormant season, nonlinearity decreases due to reduced competition from evapotranspiration and replenished water storage. We underscore that the significant variability in evapotranspiration amplifies the fluctuation of



catchment storage conditions, causing soil moisture levels to oscillate between drier and wetter states. This alternation leads to the occurrence of both very small and very large events, which are characteristic of heavy-tailed flood behavior.

This dynamic is particularly pronounced in the continental United States (panel b), where is characterized by a wide range of geography and diverse temperate and continental climates. The number of inferred heavy-tailed cases can increase by 50 % from spring to autumn. In the Atlantic Europe (panels c and d), heavy-tailed behavior is relatively prevalent and shows no significant distinction from spring to autumn, but still experiences a noticeable decrease in winter, likely due to lower temperatures and evapotranspiration. Northern Europe (panel e) presents different patterns due to varying controls on runoff generation. A slight increase in heavy-tailed cases during the winter is observed, which could be attributed to a relatively higher contribution of rainfall-driven flood events during a season when snowmelt-driven events are less common.

We delve into the seasonal characteristics of this behavior further by combining the regional patterns based on climate classification.

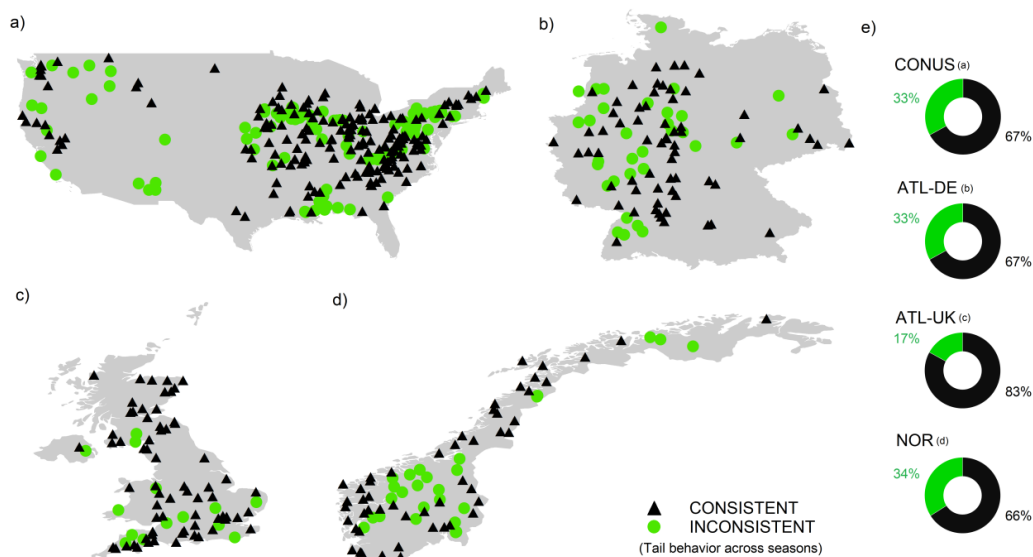
We find that the grouping based on their distinct patterns of seasonality (Figure 7a) closely aligns with the grouping based on the analysis of dominant patterns throughout the year (Figure 4 and Table 1). Regions (red area in Figure 7a corresponded to the heavy-tailed group in Table 1) characterized by uneven rainfall distribution throughout the year based on the Köppen classification (see Table S1 in the supporting information), leading to pronounced fluctuations between drier and wetter soil states, combined with higher evapotranspiration rates (indicated by warm to hot temperatures), tend to exhibit a dominance of heavy-tailed behavior in their hydrological responses across all seasons. In regions represented by the white area in Figure 7a (corresponding to the neutral group in Table 1), unlike the former group (red area), the rainfall pattern does not favor the emergence of heavy-tailed behavior as it is more evenly distributed in time. However, strong evapotranspiration, as depicted in Figure 7b, characterizes these areas. The increased evapotranspiration during the growing seasons and decreased during the dormant seasons may be mainly responsible for the seasonality of flood tail behavior in these areas. Regions represented by the blue area in Figure 7a (corresponding to the nonheavy-tailed group in Table 1) still exhibit dynamics in evapotranspiration across seasons, but the amounts are comparably low (Figure 7b). In these regions, runoff generation is primarily influenced by snow dynamics, and most runoff results from snowmelt during the growing seasons, driven by energy availability. Previous study (Santos et al., 2018) has found that such a flood generation process tends to display close-to-linear hydrological responses. These findings support the proposed mechanism of heavy-tailed flood behavior concluded in the spatial analyses and further demonstrate the pivotal effect played by the variation of evapotranspiration and catchment storage on the emergence of heavy-tailed flood behavior.

We acknowledge that the hydroclimatic factors analyzed in this study may not account for all cases, as observed in regions classified as Cfa and Cfb, where the former has higher temperatures but fewer heavy-tailed case studies compared to the latter. This discrepancy could be attributed to either the uncertainty in inferring heavy-tailed floods through recession exponents or the presence of additional factors or mechanisms influencing flood tail behavior in these regions. It is crucial to note that most catchments classified as Cfb in our dataset are primarily from the UK, while those classified as Cfa are mostly from the Southeast US. Indeed, extreme floods are prevalent in the UK (European Environmental Agency, 2010; Robson, 2002), aligning with the inference based on our analysis of recession exponents. One of the primary causes of floods in the UK is suggested to be extreme or storm-related heavy rainfall (Osborn et al., 2000; Huntingford et al., 2014), which has been identified to some extent as a factor contributing to the emergence of heavy-tailed flood behavior (e.g., McCuen and Smith; Macdonald et al., 2022) but has not been explicitly included in the analyses of this study.

In summary, while heavy-/nonheavy-tailed behavior is generally consistent across seasons, there is a certain probability for cases to exhibit seasonality. This seasonality of inferred heavy-tailed behavior shows a dynamic pattern of increasing during the growing season and decreasing during the dormant season. Regions with pronounced



570 temperature variations across seasons, particularly with higher temperature in summer, tend to display such dynamics and highlight the role of evapotranspiration in catchments in driving this seasonality.



575

Figure 5. Consistency of inferred flood tail behavior across seasons. (a) 290 catchments in CONUS. (b) 98 catchments in ATL-DE. (c) 81 catchments in ATL-UK. (d) 79 catchments in NOR. (e) Percentage of consistent and inconsistent catchments in each country.

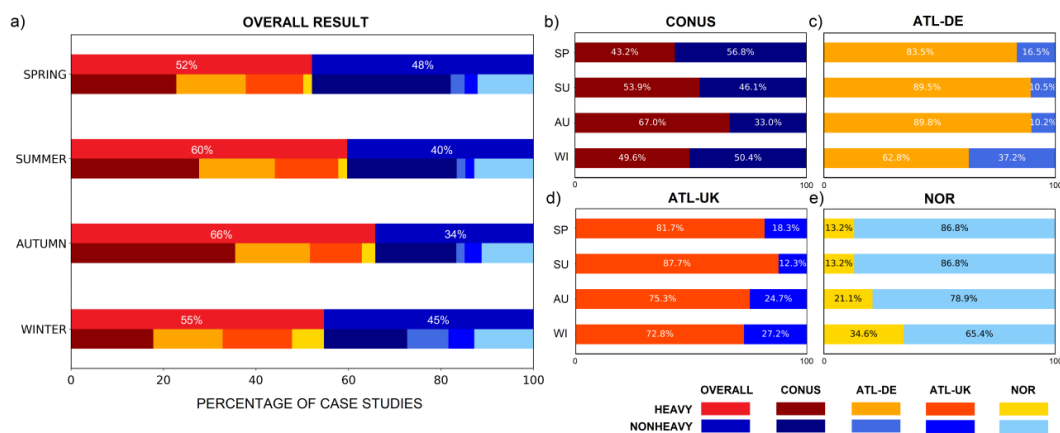


Figure 6. Seasonal variations in the percentage of inferred flood tail behavior between heavy and nonheavy case studies. (a) The aggregated results encompass all study regions, while the second line provides a breakdown by country. In total, there are



1,997 case studies composed by 540 in spring, 520 in summer, 543 in autumn, and 394 in winter. (b)-(e) Results for each study region (see Table A1 for detailed case numbers across seasons in each region).

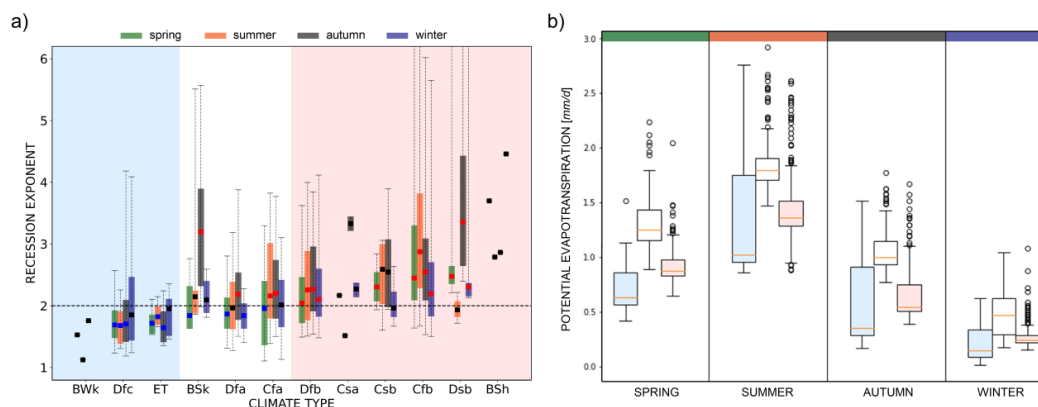


Figure 7. Seasonal variations in recession exponents (inferred flood tail behavior) and potential evapotranspiration across diverse climate regions. a) Seasonality of flood tail behavior. Case studies grouped by climate regions based on seasons. Medians of recession exponents in each group are compared with a value of two using Wilcoxon signed-rank test (significance level: 0.05). Red squares indicate significantly heavy-tailed (recession exponents > 2) groups, blue squares indicate significantly nonheavy-tailed (recession exponents < 2) groups, and black squares denote insignificance. Climate regions are categorized as follows: the red area denotes regions with prominent heavy tails across seasons, the blue area denotes regions with prominent nonheavy tails across seasons, and the white area denotes regions with significant seasonality in flood tail behavior. b) Seasonality of derived potential evapotranspiration (Zomer and Trabucco, 2022) as a function of the seasonality characteristic of flood tail behavior.

4.4 Factors associated with catchment scales and their role in flood tail behavior

It remains unclear how flood tail behavior varies across catchment scales and what the underlying drivers and mechanisms are (Merz et al., 2022). We employ catchment nonlinearity, represented by recession exponents, to explore the influence of catchment scales on flood tail behavior, as depicted in Figure 8. We utilize the categorization of regions characterized by distinct controls on flood tail behavior, primarily influenced by characteristic runoff generation processes (as three groups identified in Figure 7), to elucidate the underlying mechanisms. Case studies are categorized into bins based on catchment areas, with the median values represented by squares, interquartile intervals depicted by vertical bars, and catchment area ranges indicated by horizontal dashed bars. Panels a, b, c, and d present results for all regions, regions exhibiting significant heavy tails across seasons, regions with a neutral propensity and seasonal variations, and regions displaying pronounced nonheavy tails across seasons, respectively. Each panel comprises a total of 30 bins, with approximately 67, 33, 24, and 10 case studies in panels a, b, c, and d, respectively (with minor variations due to rounding).

From the perspective of all case studies (Figure 8a), the pattern appears somewhat unclear. Apart from the case studies involving extremely small and large catchment areas, there seems to be a decrease in nonlinearity as catchment areas increase. Nevertheless, the relationship is rather weak and lacks clarity. These findings align with previous discussions on this matter (e.g., Merz and Blöschl, 2009; Villarini and Smith, 2010; Smith et al., 2018), which have suggested a relatively weak inverse correlation between catchment area and the occurrence of heavy-tailed flood behavior.

However, we can evidently clarify this relationship by considering the distinct runoff generation processes recognized in different regions. Panel b illustrates that catchment area plays no significant role in catchment nonlinearity in regions characterized by prominent heavy tails. Whereas a clear inverse relationship between nonlinearity and catchment area is shown in panel c, representing regions characterized by a neutral propensity for heavy and nonheavy



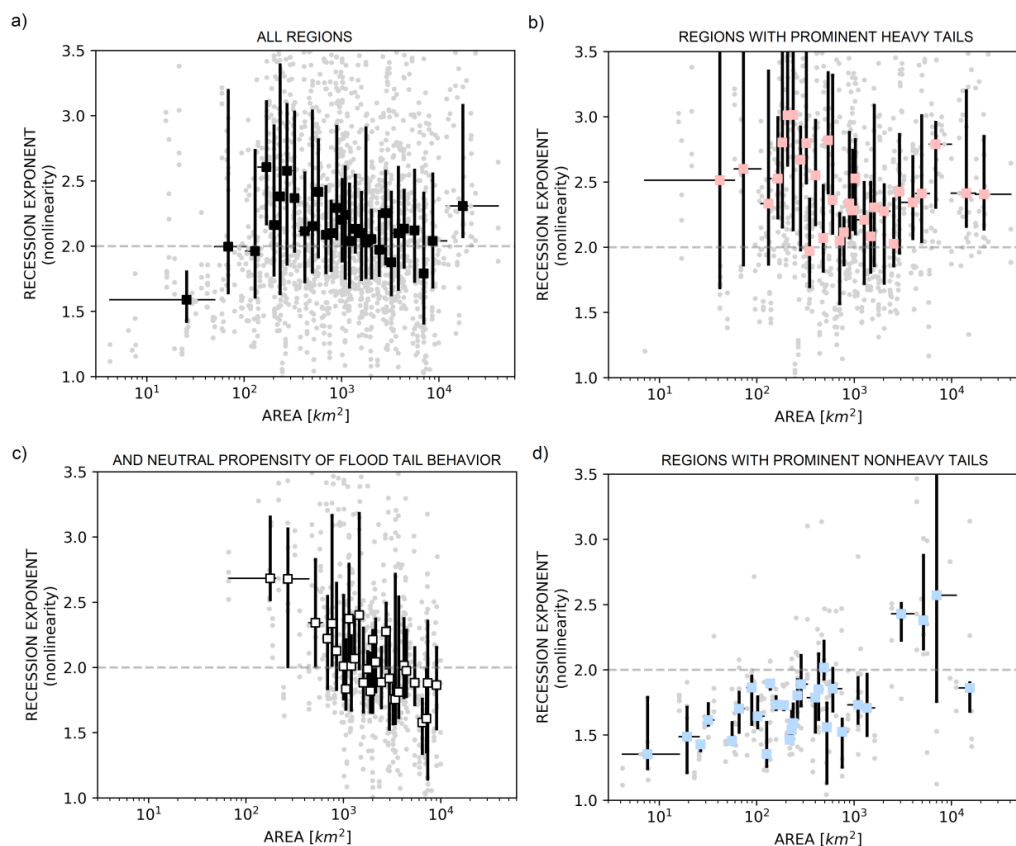
tails. In contrast, a proportional relationship between nonlinearity and catchment area is identified in panel d, representing regions characterized by prominent nonheavy tails.

615 As shown by the previous sections, nonlinearity in neutral regions is primarily driven by high evapotranspiration
facilitated by high temperatures. When the catchment area increases, it has a higher chance of encompassing diverse
terrain types, including areas with higher altitudes, such as mountainous regions. Increased altitude tends to result in
620 lower temperatures and evapotranspiration rates, negating the evapotranspiration variation and its impact on catchment
nonlinearity, which is the main driver of nonlinearity in this region and thus substantiates an inverse relationship
(Figure 8c). In regions with prominent heavy tails (Figure 8b), nonlinearity is generated from the interplay of uneven
rainfall and evapotranspiration dynamics, and the enlargement of catchments does not substantively change this
625 relationship. For regions with prominent nonheavy tails (Figure 8d), the underlying mechanisms are similar to the
neutral regions but work in the opposite direction due to the differently dominant mechanism. Recall that the runoff
process in this region is generally dominated by snow dynamics. The region is mainly located in high mountain or
high latitude areas. As catchments expand, more diverse terrain is encompassed, potentially introducing a mixture of
flood generation processes due to the incorporation of lowland or coastal areas. Particularly, more rain-on-snow events
or rainfall-driven events may be encompassed in a same catchment together with snowmelt-driven events (Vormoor
et al., 2016). Therefore, an increase in nonlinearity is facilitated due to the mixture of flood types, favoring the
emergence of heavier tails in flood distributions (Tarasova et al., 2020). It should be noted that the tail patterns, based



on Figure 8d, are still more likely to be nonheavy tails (i.e., recession exponents below two), even though nonlinearity indeed appears to show an increasing tendency along with catchment area.

630 These findings disentangle the relationship between flood tail behavior (inferred from catchment nonlinearity) and catchment scale, and provide a mechanistic understanding that underscores the role of variability in runoff generation processes introduced by the expansion of catchment area.



635 **Figure 8. Catchment nonlinearity as a function of catchment area.** The recession exponents, representing catchment nonlinearity, have been evenly grouped into bins based on catchment areas. The squares denote the median values, vertical bars represent the interquartile intervals of the recession exponents, and horizontal dashed bars indicate the catchment area ranges for each bin. (a) All regions (encompassing case studies, $n=1997$). (b)-(d) show case studies separately according to categorization recognized in Figure 7. (b) Regions with prominent heavy tails ($n=978$). (c) Regions with seasonality and neutral propensity of flood tail behavior ($n=733$). (d) Regions with prominent nonheavy tails ($n=286$). In each panel, there are a total of 30 bins, each containing approximately 67, 33, 24, and 10 case studies in panels a, b, c, and d, respectively (with slight variations due to rounding).
640

5 Discussion

645 We have confirmed the effectiveness of the recession exponent in identifying heavy-tailed flood behavior in case studies across study regions with varying degrees of the propensity of such behavior: heavy-tailed richness (the Atlantic Europe), neutrality (the continental United States), and nonheavy-tailed richness (Northern Europe). This validation is substantiated by power law tailed cases, widely acknowledged as representatives of heavy-tailed distributions (El Adlouni et al., 2008; Clauset et al., 2009), and supported by the significance of catchment nonlinearity



as a robust driver of heavy-tailed flood behavior (Fiorentino et al., 2007; Struthers and Sivapalan, 2007; Gioia et al., 2008; Rogger et al., 2012; Basso et al., 2015; Merz et al., 2022; Basso et al., 2023; Wang et al., 2023).

650 Our findings first indicate that regions with relatively uniform hydroclimatic conditions (the Atlantic Europe and Northern Europe) tend to exhibit a single/dominant propensity of flood tail behavior. Conversely, in regions characterized by diverse conditions (the continental United States), inferred flood tail behavior presents a balance between heavy- and nonheavy-tailed cases in terms of frequency and distribution. Climate conditions have been found shaping the catchment geomorphology (Wu et al., 2023) and river network dynamics (Ward et al., 2020) which contribute to the degree of catchment response nonlinearity (Biswal and Marani, 2010). Meanwhile, the changes in
655 flood generation processes can significantly affect the frequency of large floods (Tarasova et al., 2023), potentially altering flood tail behavior. Our findings in Figure 3e exemplify how different flood generation processes, influenced by the interplay of varied hydrometeorological and terrain conditions, result in opposite flood tail propensities.

We further identify key drivers of heavy-tailed flood behavior by conducting large scale physioclimatic analyses. Specifically, our findings reveal that regions with a pronounced propensity for heavy tails exhibit distinct
660 characteristics: the presence of a dry period and higher temperatures (as shown in Figure 4 and Table 1). This aligns with previous studies based on the mathematical analysis which associates heavier-tailed flood behavior with a lower frequency of streamflow-triggering rainfall events. Such lower frequency often results from erratic rainfall patterns and higher rates of evapotranspiration, leading to drier catchment conditions (Botter, 2010; Basso et al., 2016). In line with this theory, our large scale analysis provides evidence by showing a prevalent propensity for heavy tails in regions
665 characterized by uneven rainfall patterns throughout the year (i.e., more erratic rainfall), contributing to the presence of dry periods, along with higher potential evapotranspiration rates, as indicated by higher temperatures.

The underlying mechanism of the emergence of heavy-tailed flood behavior is attributed to variations in catchment water storage. In wetter catchments, relatively stable runoff coefficients are observed due to consistent high levels of soil moisture across events. In contrast, drier catchments exhibit larger variations in runoff coefficients between small
670 and large events (Merz and Blöschl, 2009; Viglione et al., 2009). This increased variability in runoff coefficients results in high nonlinearity of catchment responses, favoring heavy-tailed flood behavior. Previous studies have suggested the prevalence of heavy tails in drier catchments (Molnar et al., 2006; Merz and Blöschl, 2009; Guo et al., 2014). Our findings show that this mechanism is primarily driven by concurrent higher evapotranspiration and lower rainfall in summer, as well as lower evapotranspiration and higher rainfall in winter. These conditions lead to
675 variations in storage, enabling the occurrence of both very small and very large flood events, thereby resulting in heavy-tailed flood behavior. In line with this, Tarasova et al. (2018) observed clear seasonal dynamics of catchment average runoff coefficients in Germany, with higher values in wet winters and lower values in dry summers.

The seasonality of flood tail behavior has been suggested in previous studies but remains less understood (Basso et al., 2015; Smith et al., 2018; Macdonald et al., 2022). It's noteworthy that more than one-third of catchments appear
680 to exhibit inconsistent flood tail behavior across seasons (Figure 5). In these catchments, some seasons show a tendency toward nonheavy tails, while others tend to display heavy tails. Identifying these catchments and understanding the factors driving them to exhibit heavy tails is vital for hazard assessment. This understanding allows us to pinpoint catchments where extreme floods could potentially occur, even if methods solely based on annual maximum floods might estimate the flood tail as nonheavy based on annual maxima, when heavy tails can still occur
685 within a single season. We have identified that regions characterized by stronger evapotranspiration favor this seasonality of flood tail behavior, as it may lead to larger variations in water storage, particularly in the growing seasons (highlighted in white in Figure 7). This finding aligns with previous studies that have observed similar seasonal dynamics in the nonlinearity of hydrological responses (Tashie et al., 2019; Tarasova et al., 2018).

In this study, we also found that the relationship between flood tail behavior and the expansion of catchment scales can be explained by changes in catchment nonlinearity, which are influenced by distinct flood generation processes. Previous studies have presented diverse perspectives on the relationship between flood tail behavior and catchment
690 scales. While some studies have suggested that smaller catchments tend to exhibit heavier tails (e.g., Meigh et al., 1997; Pallard et al., 2009), others have noted a similar trend but with only a weak correlation (Merz and Blöschl, 2009; Villarini and Smith, 2010). Meanwhile, some studies have found no significant relationship between these two variables (Morrison and Smith, 2002; Smith et al., 2018). These studies have explored this topic without reaching a consensus, and many conclusions lack sufficient evidence and a clear understanding. In contrast, our findings (Figure
695 8) distinctly differentiate between various patterns by considering region classifications based on distinct dominant



700 flood generation processes, thereby providing a mechanistic understanding. As a catchment expands, it encompasses
more diverse terrain, which in turn facilitates a wider range of altitudes and flood types. In regions where tail behavior
is primarily influenced by evapotranspiration dynamics (Figure 8c), the presence of diverse altitudes tends to moderate
the effect of higher temperatures, reducing the influence of high evapotranspiration on the emergence of heavy tails.
705 In regions where tail behavior is primarily controlled by snowmelt (Figure 8d) (mainly composed of catchments in
Norway in this study), it has been shown that larger catchments are more likely to encompass a mix of flood types,
including snowmelt-driven and rainfall-driven floods (Vormoor et al., 2016). Merz et al. (2022) suggested that heavier-
tailed behavior in rainfall-driven floods tends to dominate in such mixed conditions. Our findings support this
hypothesis by demonstrating an increase in tail heaviness as catchment area enlarges. In regions where heavy tails are
pronounced due to the strong nonlinearity resulting from the interplay of uneven rainfall and high evapotranspiration,
there is no significant relationship between catchment nonlinearity and catchment area (Figure 8b). This lack of
710 relationship may be because the expansion of the catchment area does not appear to significantly enhance or reduce
this interplay.

To summarize the findings and underscore the contributions of this study, we benchmark them against the existing
hypotheses proposed in the state-of-the-art review of heavy-tailed flood distributions (Merz et al., 2022). These
hypotheses (highlighted in italics) provide a framework for understanding the factors influencing flood tail behavior,
and our study sheds light on which of these hypotheses receive stronger support or require further refinement. We
715 acknowledge that this summary does not cover all the hypotheses proposed in the review due to the scope of this study.
Instead, it primarily focuses on the compartments of the atmosphere and catchment:

*“Hypothesis 2 (of the review paper): The Characteristic Flood Generation Process Shapes the Upper Flood Tail
Catchments.”* While previous studies have hinted at the possibility that regions where flood generation is dominated
720 by rainfall-driven floods tend to exhibit heavier-tailed flood behavior compared to regions dominated by snowmelt
(Bernardara et al., 2008; Thorarindottir et al., 2018), more explicit process explanations are desired. In line with this
hypothesis, we present further evidence showing that the specific nonlinearity inherent in each flood generation
process is the primary driver of flood tail behavior. Specifically, we show that in snowmelt-dominated regions, such
as the case studies in Norway, hydrological responses closely resemble linear behavior and thus floods tend to exhibit
725 pronounced nonheavy-tailed behavior. Conversely, heavy-tailed floods are more prominent in regions like the UK,
where hydrological responses display nonlinearity (as indicated by recession exponents above two). In these areas,
flood generation processes are primarily driven by rainfall events. Furthermore, our study reveals that flood generation
processes are significantly influenced by the interplay between regional terrain and meteorological features. These
factors, in turn, impact the nonlinearity of hydrological responses and can determine the occurrence of heavy or
nonheavy tails in flood distributions (Figure 3e).

730 *“Hypothesis 3: Mixture of Flood Event Types Generates Heavy Tails.”* One argument presented in this hypothesis is
that heavy tails may arise from the presence of a flood type displaying heavy-tailed behavior within a mixture of
processes (Morrison and Smith, 2002; Villarini and Smith, 2010). However, studies exploring the relationship between
the mixture of flood types and flood tails have been lacking. Our research addresses this gap by demonstrating that in
regions primarily characterized by nonheavy-tailed floods, driven mainly by snowmelt, the tail heaviness increases as
735 catchment areas expand. This increase is likely attributed to the incorporation of additional flood types, especially
those associated with rainfall processes occurring in lowland and coastal areas, as catchment areas expand. Thus, our
findings provide evidence that supports this hypothesis.

“Hypothesis 4: Non-Linear Response to Precipitation Causes Heavy Flood Tails.” Studies have consistently
740 highlighted the significance of nonlinearity in hydrological processes within catchments as a key determinant in the
emergence of heavy-tailed flood behavior (e.g., Struthers and Sivapalan, 2007; Rogger et al., 2012; Basso et al., 2015).
In our research, we contribute by introducing a quantitative approach that employs hydrograph recession exponents
as a measure of nonlinearity in flood tail analyses and validate its effectiveness in identifying heavy-tailed flood
behavior in a large scale analysis. While nonlinearity has long been acknowledged as a contributing factor, our works
uniquely utilizes this driver as a reliable index by establishing a specific recession exponent threshold that robustly
745 discriminates heavy-tailed distributions, characterized by power-law tails, from nonheavy ones, offering a valuable
tool to the field. Furthermore, our large scale analysis identifies rainfall unevenness and high temperatures as crucial
drivers behind the observed nonlinearity in flood responses. Specifically, they intensify catchment soil dryness and



amplify water balance storage variations, thereby facilitating both very small and very large runoff events, translating into heavy-tailed flood behavior.

750 *“Hypothesis 5: Drier Catchments Have Heavier Flood Tails Due To Interaction of Water Balance Processes.”* In alignment with previous studies that suggest the water balance processes in drier catchments contribute to the emergence of heavy-tailed flood behavior (e.g., Molnar et al., 2006; Merz and Blöschl, 2009; Guo et al., 2014), we emphasize the critical interplay between uneven rainfall and evapotranspiration dynamics in facilitating these processes and shaping such the behavior. Specifically, our findings show that heavy-tailed flood behavior is more
755 likely to occur in catchments characterized by lower rainfall and higher evapotranspiration in one season (e.g., summer), contrasted with more rainfall and lower evapotranspiration in another season (e.g., winter). When one of these conditions is lacking, heavy-tailed behavior may be less pronounced. For example, regions classified as BSh and BSk, both of which exhibit semi-arid characteristics based on their rainfall patterns, exhibit differences in the prevalence of heavy-tailed cases. BSk regions, despite their semi-arid status, exhibit fewer pronounced heavy-tailed cases due to colder temperatures (Table 1) and only show a higher rate of heavy-tailed cases during the summer (Figure
760 7). This interplay highlights the importance of considering the seasonality of flood tail behavior, particularly in regions that do not experience significant dry periods based on their rainfall patterns. In such regions, heavy tails are still likely to occur in seasons with higher evapotranspiration rates (indicated by the white area in Figure 7).

765 *“Hypothesis 6: Smaller Catchments Have Heavier Flood Tails Due To Less Pronounced Spatial Aggregation Effects.”* A commonly debated question among hydrologists is whether the roles identified in large catchments are applicable to smaller ones, and vice versa. This issue has also arisen in discussions regarding flood tail heaviness, but evidence on the matter has been scattered. While smaller catchments have been suggested to exhibit heavier tails (Meigh et al., 1997; Pallard et al., 2009), previous research has revealed weak (Merz and Blöschl, 2009; Villarini and Smith, 2010) to no (Morrison and Smith, 2002; Smith et al., 2018) correlations between catchment size and tail heaviness. Our
770 findings (Figure 8) help clarify the relationship between catchment nonlinearity (used as an indicator of tail heaviness) and catchment sizes. We observe distinct patterns among regions characterized by strong, neutral, and weak conditions of heavy tail behavior. These findings underscore the importance of considering the dominant flood generation processes in each region and elucidate how catchment size interacts with flood tail behavior by influencing these dominant processes—either amplifying, reducing, or having no significant effect.

775 6 Conclusions

We analyze common streamflow dynamics to infer heavy-tailed flood behavior by employing a recently developed index of tail heaviness, namely the hydrograph recession exponent. The wide-ranging dataset allows for unveiling spatial and seasonal patterns of flood tail behavior, and to construct a geography of heavy-tailed flood distributions. We analyze and discuss the underlying influences of hydroclimatic settings on this geographical patterns, as
780 represented by Köppen climate characteristics. The main findings of this study can be summarized as follows:

- 785 1. **Capability of Recession Exponents for Detecting Heavy-Tailed Flood Behavior:** The capability of this index to discern between case studies which display heavy-tailed flood distributions and those exhibit nonheavy-tailed behavior is validated by using empirical data from catchments across an extensive dataset covering the Atlantic Europe, Northern Europe, and the continental United States. This extensive analysis provides a well-rounded evaluation due to the inclusion of regions with divergent conditions, such as rainfall-driven floods (the Atlantic Europe and the continental United States) versus snowmelt-driven floods (Northern Europe), as well as regions characterized by single/dominant hydroclimates (the Atlantic and Northern Europe) versus those with mixed hydroclimates (the continental United States).
- 790 2. **Regional Propensity for Heavy-Tailed Flood Behavior:** The Atlantic Europe are characterized by a propensity for heavy-tailed flood behavior, which is prevalent in these regions. Conversely, a tendency for nonheavy-tailed flood behavior is predominant in Northern Europe under current hydroclimatic conditions, as indicated by the degree of catchment nonlinearity in each region. The continental United States exhibits a mixture of heavy- and nonheavy-tailed behavior. This is likely the results of overarching climatic characteristics, which also shape river network morphology, interacting with diverse regional physioclimatic settings. We emphasize that the relatively
795 more uniform climates in the Atlantic and Northern European regions covered in this study contribute to a dominant presence of heavy or nonheavy-tailed behaviors in these countries, while the continental United States encompasses more complex patterns due to more diverse hydroclimatic conditions.



- 800 3. **Factors Influencing Heavy-Tailed Flood Behavior:** The presence of simultaneous dry periods (defined by uneven rainfall throughout the year) and higher temperatures emerge as the pivotal conditions favoring heavy-tailed flood behavior. Drier catchments alter the runoff generation process, resulting in higher nonlinearity of catchment responses, while higher temperatures elevate evapotranspiration rates, enhancing nonlinearity but also maintaining atmospheric moisture preventing precipitation limitations. The absence of either condition diminishes the prevalence of heavy-tailed flood behavior. More generalized climate categorizations like Arid, Temperate, and Continental exhibit minimal influence on our results.
- 805 4. **Seasonality of Flood Tail Behavior:** We contribute to a better understanding of the seasonality of flood tail behavior. Around two-thirds of catchments exhibit consistent behavior across seasons, with the remaining one-third demonstrating seasonality. Heavy-tailed flood behavior is more likely during the growing season (spring to autumn) and diminishes during the dormant season (autumn to winter). These findings hint at the role of temperature-driven evapotranspiration dynamics for the emergence of heavy-tailed flood behavior, which are particularly important in regions which do not experience simultaneous dry conditions and high temperatures.
- 810 5. **Influences of Catchment Area on Flood Tail Behavior:** We elucidate that the impacts of catchment size on flood tail behavior are primarily contingent on the dominant flood generation processes within each region. Specifically, the expansion of catchment area tends to have three distinct effects: (1) It diminishes tail heaviness in regions with moderate nonlinearity, characterized by strong evapotranspiration dynamics and relatively even rainfall throughout the year. This reduction is attributed to the smoothing of evapotranspiration variations. (2) Conversely, in regions with low nonlinearity, characterized by snowfall dynamics, increasing catchment area intensifies tail heaviness. This effect results from the inclusion of diverse flood types, particularly rainfall-driven floods. (3) In regions with high nonlinearity, characterized by simultaneous strong evapotranspiration dynamics and uneven rainfall throughout the year, catchment size expansion appears to have no significant impact on tail heaviness. This lack of effect is likely due to the absence of significant influence on rainfall patterns, which are critical in determining the presence of drier soil conditions.
- 815
- 820

We propose that a key mechanism driving the emergence of heavy-tailed flood behavior is the temporal variability in catchment storage, primarily induced by simultaneous high evapotranspiration rates and drier soil conditions. This variation in storage can lead to the occurrence of both very small and very large flood events, ultimately resulting in heavy-tailed flood behavior. In contrast, when the catchment remains consistently wet or dry, the magnitude of generated floods tends to fall within a similar range, leading to nonheavy tails in the distribution. It's important to emphasize that this mechanism is influenced by seasonality and catchment sizes, both of which play a role in shaping the variability in catchment storage.

825

Acknowledgments

830 This work is supported by the Deutsche Forschungsgemeinschaft (DFG, German Research Foundation) through Project number 421396820 "Propensity of rivers to extreme floods: climate-landscape controls and early detection (PREDICTED)" and Research Group FOR 2416 "Space-Time Dynamics of Extreme Floods (SPATE)". We also acknowledge the financial support provided by the Helmholtz Centre for Environmental Research - UFZ. The manuscript and supporting information contain all the necessary details to replicate the results.

835 Data Availability Statement

We express our gratitude to the following organizations for providing the discharge data: the Bavarian State Office of Environment (LfU) in Germany (<https://www.gkd.bayern.de/de/fluesse/abfluss>, Bayerisches Landesamt für Umwelt, 2022), the Global Runoff Data Centre (GRDC) prepared by the Federal Institute for Hydrology (BfG) in the UK and Norway (<http://www.bafg.de/GRDC/EN>, Bundesanstalt für Gewässerkunde, 2023), and the National Oceanic and Atmospheric Administration (NOAA) Office of Global Programs (MOPEX) in the US (<http://hydrology.nws.noaa.gov/pub/gcip>, Schaake et al., 2006). We obtained the digital elevation model from the Shuttle Radar Topography Mission (SRTM) (<https://cgiarcsi.community/data/srtm-90m-digital-elevation-database-v4-1/>, Jarvis et al., 2022). Köppen climate classification were sourced from the high-resolution present-day Köppen climate map (<https://doi.org/10.1038/sdata.2018.214>, Beck et al., 2018). Derived potential evapotranspiration were sourced from the high-resolution map (<https://doi.org/10.1038/s41597-022-01493-1>, Zomer and Trabucco, 2022). The dataset of dams used in this study is available from the GeoDAR v.1.0 (<https://doi.org/10.5281/zenodo.6163413>,

840

845



Wang et al., 2022). For characteristics of separated rainfall-runoff events for each streamflow gauge used in the analysis, please refer to Data Set S1 of Tarasova et al., 2018 (https://doi.org/10.1029/2018WR022588).

Appendix A Information on Study Regions

850 **Table A1. Daily Hydrological Data Information**

Region	The Atlantic Europe		Northern Europe	The Continental United States
	Germany	UK	Norway	
Gauge Number	98	82	82	313
Catchment Size [km ²]	110 – 23,843 (median: 1,195)	15 – 9,948 (median: 283)	4 – 40,504 (median: 234)	66 – 9,935 (median: 1,769)
Streamflow Record Length [year]	35 – 63 (median: 58)	50 – 138 (median: 59)	50 – 148 (median: 96)	24 – 55 (median: 55)
Streamflow Record Duration	1951 – 2013	1883 – 2021	1871 – 2019	1948 – 2002
Number of Case Study (spring / summer / autumn / winter)	386 (97 / 96 / 98 / 95)	325 (82 / 81 / 81 / 81)	306 (76 / 76 / 76 / 78)	980 (285 / 267 / 288 / 140)

Author contributions

Hsing-Jui Wang: Conceptualization (lead); Data curation (lead); Formal analysis (lead); Methodology (lead); Investigation (lead); Software (lead); Visualization (lead); Writing – original draft (lead); Writing – review and editing (equal).

855 Ralf Merz: Conceptualization (support); Formal analysis (equal), Methodology (support); Investigation (support); Supervision (lead); Visualization (support); Writing – review and editing (equal).

Stefano Basso: Conceptualization (support); Formal analysis (equal); Methodology (lead); Investigation (lead); Software (support); Supervision (lead); Visualization (support); Writing – review and editing (equal).

Declaration of Competing Interest

860 The authors declare that they have no known competing financial interests or personal relationships that could have appeared to influence the work reported in this paper.



References

- Allen, R. G., Pereira, L. S., Raes, D., and Smith, M.: Crop evapotranspiration — guidelines for computing crop water requirements — FAO Irrigation and drainage paper 56. Food and Agriculture Organization. Rome. Retrieved from <http://www.kimberly.uidaho.edu/water/fao56/fao56.pdf>, 1998.
- Alstott, J., Bullmore, E., and Plenz, D.: Powerlaw: A python package for analysis of heavy-tailed distributions. *PLoS ONE*, 9(1). <https://doi.org/10.1371/journal.pone.0085777>, 2014.
- Arai, R., Toyoda, Y., and Kazama, S.: Runoff recession features in an analytical probabilistic streamflow model. *Journal of Hydrology*, 597, 125745. <https://doi.org/10.1016/j.jhydrol.2020.125745>, 2020.
- Barnes, B. S.: The structure of discharge-recession curves. *Eos Trans. AGU*, 20(4), 721–725. <https://doi.org/10.1029/TR020i004p00721>, 1939.
- Basso, S., Botter, G., Merz, R., and Miniussi, A.: PHEV! The PHysically-based Extreme Value distribution of river flows. *Environmental Research Letters*, 16, 124065. <https://doi.org/10.1088/1748-9326/ac3d59>, 2021.
- Basso, S., Schirmer, M., and Botter, G.: On the emergence of heavy-tailed streamflow distributions. *Advances in Water Resources*, 82, 98–105. <https://doi.org/10.1016/j.advwatres.2015.04.013>, 2015.
- Basso, S., Schirmer, M., and Botter, G.: A physically based analytical model of flood frequency curves. *Geophysical Research Letters*, 43(17), 9070–9076. <https://doi.org/10.1002/2016GL069915>, 2016.
- Basso, S., Merz, R., Tarasova, L., and Miniussi, A.: Extreme flooding controlled by stream network organization and flow regime. *Nature Geoscience*, 16(April), 339–343. <https://doi.org/10.1038/s41561-023-01155-w>, 2023.
- Bayerisches Landesamt für Umwelt.: Abfluss Bayern, Bayerisches Landesamt für Umwelt [dataset]. Retrieved August 26, 2022, from <https://www.gkd.bayern.de/de/fluesse/abfluss>, 2022.
- Beck, H. E., Zimmermann, N. E., McVicar, T. R., Vergopolan, N., Berg, A., and Wood, E. F.: Present and future Köppen-Geiger climate classification maps at 1-km resolution. *Scientific Data*, 5, 180214. [dataset]. <https://doi.org/10.1038/sdata.2018.214>, 2018.
- Bernardara, P., Schertzer, D., Sauquet, E., Tchiguirinskaia, I., and Lang, M.: The flood probability distribution tail: How heavy is it? *Stochastic Environmental Research and Risk Assessment*, 22(1), 107–122. <https://doi.org/10.1007/s00477-006-0101-2>, 2008.
- Bevere, L. and Remondi, F.: Natural catastrophes in 2021: the floodgates are open. Swiss Re Institute sigma research, <https://www.swissre.com/institute/research/sigma-research/sigma-2022-01.html> (last access: 8 May 2023), 2022.
- Biswal, B. and Kumar, D. N.: Study of dynamic behaviour of recession curves. *Hydrological Processes*, 784–792. <https://doi.org/10.1002/hyp.9604>, 2014.
- Biswal, B. and Marani, M.: Geomorphological origin of recession curves. *Geophysical Research Letters*, 37(24), 1–5. <https://doi.org/10.1029/2010GL045415>, 2010.
- Botter, G.: Stochastic recession rates and the probabilistic structure of stream flows. *Water Resources Research*, 46(12). <https://doi.org/10.1029/2010WR009217>, 2010.
- Botter, G., Basso, S., Porporato, A., Rodriguez-Iturbe, I., and Rinaldo, A.: Natural streamflow regime alterations: Damming of the Piave river basin (Italy). *Water Resources Research*, 46(6), 1–14. <https://doi.org/10.1029/2009WR008523>, 2010.



- 900 Botter, G., Peratoner, F., Porporato, A., Rodriguez-Iturbe, I., and Rinaldo, A.: Signatures of large-scale soil moisture dynamics on streamflow statistics across U.S. climate regimes. *Water Resources Research*, 43(11), 1–10. <https://doi.org/10.1029/2007WR006162>, 2007a.
- Botter, G., Porporato, A., Rodriguez-Iturbe, I., and Rinaldo, A.: Basin-scale soil moisture dynamics and the probabilistic characterization of carrier hydrologic flows: Slow, leaching-prone components of the hydrologic response. *Water Resources Research*, 43(2), 1–14. <https://doi.org/10.1029/2006WR005043>, 2007b.
- 905 Botter, G., Porporato, A., Rodriguez-Iturbe, I., and Rinaldo, A.: Nonlinear storage-discharge relations and catchment streamflow regimes. *Water Resources Research*, 45(10), 1–16. <https://doi.org/10.1029/2008WR007658>, 2009.
- Brutsaert, W. and Nieber, J. L.: Regionalized drought flow hydrographs from a mature glaciated plateau. *Water Resources Research*, 13(3), 637–643. <https://doi.org/10.1029/WR013i003p00637>, 1977.
- 910 Bundesanstalt für Gewässerkunde.: Global Runoff Database, Bundesanstalt für Gewässerkunde [data set], <https://www.bafg.de/GRDC/EN> (last access: 29 August, 2022), 2022.
- Cai, Y. and Hames, D.: Minimum sample size determination for generalized extreme value distribution. *Communications in Statistics: Simulation and Computation*, 40(1), 87–98. <https://doi.org/10.1080/03610918.2010.530368>, 2010.
- 915 Ceola, S., Botter, G., Bertuzzo, E., Porporato, A., Rodriguez-Iturbe, I., and Rinaldo, A.: Comparative study of ecohydrological streamflow probability distributions. *Water Resources Research*, 46(9), 1–12. <https://doi.org/10.1029/2010WR009102>, 2010.
- Chen, B. and Krajewski, W.: Analysing individual recession events: sensitivity of parameter determination to the calculation procedure. *Hydrological Sciences Journal*, 61(16), 2887–2901. <https://doi.org/10.1080/02626667.2016.1170940>, 2016.
- 920 Clauset, A., Shalizi, C. R., and Newman, M. E. J.: Power-law distributions in empirical data. *SIAM Review*, 51(4), 661–703. <https://doi.org/10.1137/070710111>, 2009.
- Cunderlik, J. M. and Burn, D. H.: Utilisation d’une information sur le régime des crues dans une analyse fréquentielle régionale des crues. *Hydrological Sciences Journal*, 47(1), 77–92. <https://doi.org/10.1080/02626660209492909>, 2002.
- 925 Doulatyari, B., Betterle, A., Basso, S., Biswal, B., Schirmer, M., and Botter, G.: Predicting streamflow distributions and flow duration curves from landscape and climate. *Advances in Water Resources*, 83, 285–298. <https://doi.org/10.1016/j.advwatres.2015.06.013>, 2015.
- Dralle, D. N., Karst, N. J., Charalampous, K., Veenstra, A., and Thompson, S. E.: Event-scale power law recession analysis: Quantifying methodological uncertainty. *Hydrology and Earth System Sciences*, 21(1), 65–81. <https://doi.org/10.5194/hess-21-65-2017>, 2017.
- 930 Duan, Q., Schaake, J., Andréassian, V., Franks, S., Goteti, G., Gupta, H. V., Gusev, Y.M., Habets, F., Hall, A., Hay, L., Hogue, T., Huang, M., Leavesley, G., Liang, X., Nasonova, O.N., Noilhan, J., Oudin, L., Sorooshian, S., Wagener, T., and Wood, E.F.: Model Parameter Estimation Experiment (MOPEX): An overview of science strategy and major results from the second and third workshops. *Journal of Hydrology*, 320(1), 3–17. <https://doi.org/10.1016/j.jhydrol.2005.07.031>, 2006
- 935



- Durrans, S. R., Eiffe, M. A., Thomas, W. O., and Goranflo, H. M.: Joint Seasonal /Annual Flood Frequency Analysis. *Journal of Hydrologic Engineering*, 8(4), 181–189. [https://doi.org/10.1061/\(asce\)1084-0699\(2003\)8:4\(181\), 2003](https://doi.org/10.1061/(asce)1084-0699(2003)8:4(181), 2003).
- 940 El Adlouni, S., Bobée, B., and Ouarda, T. B. M. J.: On the tails of extreme event distributions in hydrology. *Journal of Hydrology*, 355(1–4), 16–33. <https://doi.org/10.1016/j.jhydrol.2008.02.011>, 2008.
- European Environmental Agency: Mapping the impacts of natural hazards and technological accidents in Europe An overview of the last decade. Publications Office of the European Union. <https://doi.org/10.2800/62638>, 2010.
- Farquharson, F. A. K., Meigh, J. R., and Sutcliffe, J. V.: Regional flood frequency analysis in arid and semi-arid areas. *Journal of Hydrology*, 138(3–4), 487–501. [https://doi.org/10.1016/0022-1694\(92\)90132-F](https://doi.org/10.1016/0022-1694(92)90132-F), 1992.
- 945 Fick, S. E. and Hijmans, R. J.: WorldClim 2 new 1-km spatial resolution climate surfaces for global land areas.pdf.crdownload. *International Journal of Climatology*, 37, 4302–4315. <https://doi.org/10.1002/joc.5086>, 2017.
- Fiorentino, M., Manfreda, S., and Iacobellis, V.: Peak runoff contributing area as hydrological signature of the probability distribution of floods. *Advances in Water Resources*, 30(10), 2123–2134. <https://doi.org/10.1016/j.advwatres.2006.11.017>, 2007.
- 950 Fischer, S. and Schumann, A.: Robust flood statistics: comparison of peak over threshold approaches based on monthly maxima and TL-moments. *Hydrological Sciences Journal*, 61(3), 457–470. <https://doi.org/10.1080/02626667.2015.1054391>, 2016.
- 955 Gaume, E.: On the asymptotic behavior of flood peak distributions. *Hydrology and Earth System Sciences*, 10(2), 233–243. <https://doi.org/10.5194/hess-10-233-2006>, 2006.
- Gioia, A., Iacobellis, V., Manfreda, S., and Fiorentino, M.: Runoff thresholds in derived flood frequency distributions. *Hydrology and Earth System Sciences*, 12(6), 1295–1307. <https://doi.org/10.5194/hess-12-1295-2008>, 2008.
- Gumbel, E. J.: *Statistics of Extremes*. Columbia University Press. <https://doi.org/doi:10.7312/gumb92958>, 1958.
- 960 Guo, J., Li, H.-Y., Leung, L. R., Guo, S., Liu, P., and Sivapalan, M.: Links between flood frequency and annual water balance behaviors: A basis for similarity and regionalization. *Water Resources Research*, 50, 937–953. <https://doi.org/http://dx.doi.org/10.1002/2013WR014374>, 2014.
- Hosking, J. R. M.: L-Moments: Analysis and Estimation of Distributions Using Linear Combinations of Order Statistics. *Journal of the Royal Statistical Society*, 52(1), 105–124. Retrieved from <http://www.jstor.org/stable/2345653>, 1990.
- 965 Hosking, J. R. M. and Wallis, J. R.: Parameter and quantile estimation for the generalized Pareto distribution. *Technometrics*, 29(3), 339–349. <https://doi.org/10.1080/00401706.1987.10488243>, 1987.
- Hosking, J. R. M., Wallis, J. R., and Wood, E. F.: Estimation of the generalized extreme-value distribution by the method of probability-weighted moments. *Technometrics*, 27(3), 251–261. <https://doi.org/10.1080/00401706.1985.10488049>, 1985.
- 970 Huntingford, C., Marsh, T., Scaife, A. A., Kendon, E. J., Hannaford, J., Kay, A. L., Lockwood, M., Prudhomme, C., Reynard, N. S., Parry, S., Lowe, J. A., Screen, J. A., Ward, H. C., Roberts, M., Stott, P. A., Bell, V. A., Bailey, M., Jenkins, A., Legg, T., Otto, F. E. L., Massey, N., Schaller, N., Slingso, J., and Allen, M. R.: Potential influences



- on the United Kingdom's floods of winter 2013/14. *Nature Climate Change*, 4(9), 769–777.
975 <https://doi.org/10.1038/nclimate2314>, 2014.
- Jachens, E. R., Rupp, D. E., Roques, C., and Selker, J. S.: Recession analysis revisited: Impacts of climate on parameter estimation. *Hydrology and Earth System Sciences*, 24(3), 1159–1170. <https://doi.org/10.5194/hess-24-1159-2020>, 2020.
- Jarvis, A., Reuter, H. I., Nelson, A., and Guevara, E.: Hole-filled SRTM for the globe Version 4, CGIAR CSI [data set]. <https://cgiarcsi.community/data/srtm-90m-digital-elevation-database-v4-1> (last access: 08 August, 2022),
980 2022.
- Katz, R. W., Parlange, M. B., and Naveau, P.: Statistics of Extremes in Hydrology. *Advances in Water Resources*, 25(8-12), 1287–1304. [https://doi.org/10.1016/S0309-1708\(02\)00056-8](https://doi.org/10.1016/S0309-1708(02)00056-8), 2002.
- Klaus, A., Yu, S., and Plenz, D.: Statistical analyses support power law distributions found in neuronal avalanches.
985 *PLoS ONE*, 6(5). <https://doi.org/10.1371/journal.pone.0019779>, 2011.
- Kondor, D., Pósfai, M., Csabai, I., and Vattay, G.: Do the rich get richer? An empirical analysis of the Bitcoin transaction network. *PLoS ONE*, 9(2). <https://doi.org/10.1371/journal.pone.0086197>, 2014.
- Laio, F., Porporato, A., Fernandez-Illescas, C. P., and Rodriguez-Iturbe, I.: Plants in water-controlled ecosystems: Active role in hydrologic processes and response to water stress IV. Discussion of real cases. *Advances in Water
990 Resources*, 24(7), 745–762. [https://doi.org/10.1016/S0309-1708\(01\)00007-0](https://doi.org/10.1016/S0309-1708(01)00007-0), 2001.
- Lehner, B., Liermann, C. R., Revenga, C., Vörösmarty, C., Fekete, B., Crouzet, P., Döll, P., Endejan, M., Frenken, K., Magome, J., Nilsson, C., Robertson, J. C., Rödel, R., Sindorf, N., and Wisser, D.: High-resolution mapping of the world's reservoirs and dams for sustainable river-flow management. *Frontiers in Ecology and the Environment*, 9(9), 494–502. <https://doi.org/10.1890/100125>, 2011.
- 995 Lins, H. F.: Challenges to hydrological observations. *WMO Bulletin*, 57(1), 55–58. <https://pubs.usgs.gov/publication/70038057>, 2008.
- Macdonald, E., Merz, B., Guse, B., Wietzke, L., Ullrich, S., Kemter, M., Ahrens, B., and Vorogushyn, S.: Event and Catchment Controls of Heavy Tail Behavior of Floods. *Water Resources Research*, 58(6), 1–25. <https://doi.org/10.1029/2021wr031260>, 2022.
- 1000 Malamud, B. D.: Tails of natural hazards. *Physics World*, 17(8), 31–35. <https://doi.org/10.1088/2058-7058/17/8/35>, 2004.
- Malamud, B. D. and Turcotte, D. L.: The applicability of power-law frequency statistics to floods. *Journal of Hydrology*, 322(1–4), 168–180. <https://doi.org/10.1016/j.jhydrol.2005.02.032>, 2006.
- Mathai, J. and Mujumdar, P. P.: Use of streamflow indices to identify the catchment drivers of hydrographs.
1005 *Hydrology and Earth System Sciences*, 26(8), 2019–2033. <https://doi.org/10.5194/hess-26-2019-2022>, 2022.
- McCuen, R. H. and Smith, E.: Origin of Flood Skew. *Journal of Hydrologic Engineering*, 13(9), 771–775. [https://doi.org/10.1061/\(asce\)1084-0699\(2008\)13:9\(771\)](https://doi.org/10.1061/(asce)1084-0699(2008)13:9(771)), 2008.
- McDermott, T. K. J.: Global exposure to flood risk and poverty. *Nature Communications*, 13(1), 6–8. <https://doi.org/10.1038/s41467-022-30725-6>, 2022.



- 1010 Meigh, J. R., Farquharson, F. A. K., and Sutcliffe, J. V.: A worldwide comparison of regional flood estimation methods and climate. *Hydrological Sciences Journal*, 42(2), 225–244. <https://doi.org/10.1080/02626669709492022>, 1997.
- Mejía, A., Daly, E., Rossel, F., Javanovic, T., and Gironás, J.: A stochastic model of streamflow for urbanized basins. *Water Resources Research*, 50, 1984–2001. <https://doi.org/10.1002/2013WR014834>, 2014.
- 1015 Merz, B., Basso, S., Fischer, S., Lun, D., Blöschl, G., Merz, R., Guse, B., Viglione, A., Vorogushyn, S., Macdonald, E., Wietzke, L., and Schumann, A.: Understanding heavy tails of flood peak distributions. *Water Resources Research*, 1–37. <https://doi.org/10.1029/2021wr030506>, 2022.
- Merz, B., Blöschl, G., Vorogushyn, S., Dottori, F., Aerts, J. C. J. H., Bates, P., Bertola, M., Kemter, M., Kreibich, H., Lall, U., and Macdonald, E.: Causes, impacts and patterns of disastrous river floods. *Nature Reviews Earth and Environment*, 2(9), 592–609. <https://doi.org/10.1038/s43017-021-00195-3>, 2021.
- 1020 Merz, R. and Blöschl, G.: Process controls on the statistical flood moments - a data based analysis. *Hydrological Processes*, 23(5), 675–696. <https://doi.org/10.1002/hyp>, 2009.
- Molnar, P., Anderson, R. S., Kier, G., and Rose, J.: Relationships among probability distributions of stream discharges in floods, climate, bed load transport, and river incision. *Journal of Geophysical Research: Earth Surface*, 111(2), 1–10. <https://doi.org/10.1029/2005JF000310>, 2006.
- 1025 Morrison, J. E. and Smith, J. A.: Stochastic modeling of flood peaks using the generalized extreme value distribution. *Water Resources Research*, 38(12), 41-1-41–12. <https://doi.org/10.1029/2001wr000502>, 2002.
- Müller, M. F., Dralle, D. N., and Thompson, S. E.: Analytical model for flow duration curves in seasonally dry climates. *Water Resources Research*, 50, 5510–5531. <https://doi.org/10.1002/2014WR015301>, 2014.
- Müller, M. F., Roche, K. R., and Dralle, D. N.: Catchment processes can amplify the effect of increasing rainfall variability. *Environmental Research Letters*, 16, 084032. <https://doi.org/10.1088/1748-9326/ac153e>, 2021.
- 1030 Mushtaq, S., Miniussi, A., Merz, R., and Basso, S.: Reliable estimation of high floods: A method to select the most suitable ordinary distribution in the Metastatistical extreme value framework. *Advances in Water Resources*, 161, 104127. <https://doi.org/10.1016/j.advwatres.2022.104127>, 2022.
- Mutzner, R., Bertuzzo, E., Tarolli, P., Weijs, S. V., Nicotina, L., Ceola, S., Tomasic, N., Rodriguez-Iturbe, I., Parlange, M. B., and Rinaldo, A.: Geomorphic signatures on Brutsaert base flow recession analysis. *Water Resources Research*, 49(9), 5462–5472. <https://doi.org/10.1002/wrcr.20417>, 2013.
- 1035 Nair, J., Wierman, A., and Zwart, B.: *The Fundamentals of Heavy Tails*. Cambridge University Press and Assessment. <https://doi.org/10.1017/9781009053730>, 2022.
- Németh, L., Hübnerová, Z., and Zempléni, A.: Trend detection in GEV models. *ArXiv:1907.09435 [Stat.ME]*, 1–13. <https://doi.org/10.48550/arXiv.1907.09435>, 2020.
- 1040 Osborn, T. J., Hulme, M., Jones, P. D., and Basnett, T. A.: Observed trends in the daily intensity of United Kingdom precipitation. *International Journal of Climatology*, 20, 347–364. [https://doi.org/10.1002/\(SICI\)1097-0088\(20000330\)20](https://doi.org/10.1002/(SICI)1097-0088(20000330)20), 2000.
- Pallard, B., Castellarin, A., and Montanari, A.: A look at the links between drainage density and flood statistics. *Hydrol. Earth Syst. Sci.*, 13, 1019–1029. <https://doi.org/10.5194/hess-13-1019-2009>, 2009.
- 1045



- Papalexiou, S. M., Koutsoyiannis, D., and Makropoulos, C.: How extreme is extreme? An assessment of daily rainfall distribution tails. *Hydrol. Earth Syst. Sci.*, 17(2), 851–862. <https://doi.org/10.5194/hess-17-851-2013>, 2013.
- Papalexiou, S. M. and Koutsoyiannis, D.: Battle of extreme value distributions : A global survey on extreme daily rainfall. *Water Resources Research*, 49(1), 187–201. <https://doi.org/10.1029/2012WR012557>, 2013.
- 1050 Porporato, A., Daly, E., and Rodriguez-Iturbe, I.: Soil water balance and ecosystem response to climate change. *American Naturalist*, 164(5), 625–632. <https://doi.org/10.1086/424970>, 2004.
- Pumo, D., Viola, F., La Loggia, G., and Noto, L. V.: Annual flow duration curves assessment in ephemeral small basins. *Journal of Hydrology*, 519(PA), 258–270. <https://doi.org/10.1016/j.jhydrol.2014.07.024>, 2014.
- 1055 Robson, A. J.: Evidence for trends in UK flooding. *Philosophical Transactions of the Royal Society A*, 360, 1327–1343. <https://doi.org/10.1098/rsta.2002.1003>, 2002.
- Rogger, M., Pirkl, H., Viglione, A., Komma, J., Kohl, B., Kirnbauer, R., and Merz, R.: Step changes in the flood frequency curve : Process controls. *Water Resources Research*, 48, 1–15. <https://doi.org/10.1029/2011WR011187>, 2012.
- Roques, C., Rupp, D. E., and Selker, J. S.: Improved streamflow recession parameter estimation with attention to calculation of $-dQ/dt$. *Advances in Water Resources*, 108, 29–43. <https://doi.org/10.1016/j.advwatres.2017.07.013>, 2017.
- 1060 Rupp, D. E. and Selker, J. S.: Information, artifacts, and noise in $dQ/dt - Q$ recession analysis. *Advances in Water Resources*, 29(2), 154–160. <https://doi.org/10.1016/j.advwatres.2005.03.019>, 2006.
- Santos, A. C., Portela, M. M., Rinaldo, A., and Schaefli, B.: Analytical flow duration curves for summer streamflow in Switzerland. *Hydrol. Earth Syst. Sci.*, 22(4), 2377–2389. <https://doi.org/10.5194/hess-22-2377-2018>, 2018.
- 1065 Sartori, M. and Schiavo, S.: Connected we stand: A network perspective on trade and global food security. *Food Policy*, 57, 114–127. <https://doi.org/https://doi.org/10.1016/j.foodpol.2015.10.004>, 2015.
- Schaake, J, Cong, S, and Duan, Q.: U.S. MOPEX DATA SET [data set]. <http://hydrology.nws.noaa.gov/pub/gcip> (last access: 07 February, 2023), 2006.
- 1070 Schaefli, B., Rinaldo, A., and Botter, G.: Analytic probability distributions for snow-dominated streamflow. *Water Resources Research*, 49(5), 2701–2713. <https://doi.org/10.1002/wrcr.20234>, 2013.
- Sharma, A., Wasko, C., and Lettenmaier, D. P. (2018). If Precipitation Extremes Are Increasing, Why Aren't Floods? *Water Resources Research*, 54(11), 8545–8551. <https://doi.org/10.1029/2018WR023749>
- 1075 Smith, J. A., Cox, A. A., Baeck, M. L., Yang, L., and Bates, P.: Strange Floods: The Upper Tail of Flood Peaks in the United States. *Water Resources Research*, 54(9), 6510–6542. <https://doi.org/10.1029/2018WR022539>, 2018.
- Spearman, C.: The proof and measurement of association between two things. *American Journal of Psychology*, 15(1), 72–101. <https://doi.org/10.2307/1412159>, 1904.
- 1080 Struthers, I. and Sivapalan, M.: A conceptual investigation of process controls upon flood frequency: Role of thresholds. *Hydrology and Earth System Sciences*, 11(4), 1405–1416. <https://doi.org/10.5194/hess-11-1405-2007>, 2007.
- Tarasova, L., Basso, S., and Merz, R.: Transformation of Generation Processes From Small Runoff Events to Large Floods. *Geophysical Research Letters*, 47, e2020GL090547. <https://doi.org/10.1029/2020GL090547>, 2020.



- 1085 Tarasova, L., Basso, S., Zink, M., and Merz, R.: Exploring Controls on Rainfall-Runoff Events: 1. Time Series-Based Event Separation and Temporal Dynamics of Event Runoff Response in Germany. *Water Resources Research*, 54(10), 7711–7732. <https://doi.org/10.1029/2018WR022587>, 2018.
- Tarasova, L., Lun, D., Merz, R., Blöschl, G., Basso, S., Bertola, M., Miniussi, A., Rakovec, O., Samaniego, L., Thober, S., and Kumar, R.: Shifts in flood generation processes exacerbate regional flood anomalies in Europe. *Communications Earth and Environment*, 4(1), 49. <https://doi.org/10.1038/s43247-023-00714-8>, 2023.
- 1090 Tashie, A., Pavelsky, T., and Band, L. E.: An Empirical Reevaluation of Streamflow Recession Analysis at the Continental Scale. *Water Resources Research*, 56(1), 1–18. <https://doi.org/10.1029/2019WR025448>, 2020a.
- Tashie, A., Pavelsky, T., and Emanuel, R. E.: Spatial and Temporal Patterns in Baseflow Recession in the Continental United States. *Water Resources Research*, 56(3), 1–18. <https://doi.org/10.1029/2019WR026425>, 2020b.
- Tashie, A., Scaife, C. I., and Band, L. E.: Transpiration and subsurface controls of streamflow recession characteristics. *Hydrological Processes*, 33(19), 2561–2575. <https://doi.org/10.1002/hyp.13530>, 2019.
- 1095 Thorarindottir, T. L., Hellton, K. H., Steinbakk, G. H., Schlichting, L., and Engeland, K.: Bayesian Regional Flood Frequency Analysis for Large Catchments. *Water Resources Research*, 54(9), 6929–6947. <https://doi.org/10.1029/2017WR022460>, 2018.
- Viglione, A., Merz, R., and Blöschl, G.: On the role of the runoff coefficient in the mapping of rainfall to flood return periods. *Hydrology and Earth System Sciences*, 13(5), 577–593. <https://doi.org/10.5194/hess-13-577-2009>, 2009.
- 1100 Villarini, G. and Smith, J. A.: Flood peak distributions for the eastern United States. *Water Resources Research*, 46(6), 1–17. <https://doi.org/10.1029/2009WR008395>, 2010.
- Vogel, R. M. and Fennesse, N. M.: L moment diagrams should replace product moment diagrams. *Water Resources Research*, 29(6), 1745–1752. <https://doi.org/10.1029/93WR00341>, 1993.
- 1105 Vormoor, K., Lawrence, D., Schlichting, L., Wilson, D., and Wong, W. K.: Evidence for changes in the magnitude and frequency of observed rainfall vs. snowmelt driven floods in Norway. *Journal of Hydrology*, 538, 33–48. <https://doi.org/10.1016/j.jhydrol.2016.03.066>, 2016.
- Wang, H., Merz, R., Yang, S., Tarasova, L., and Basso, S.: Emergence of heavy tails in streamflow distributions: the role of spatial rainfall variability. *Advances in Water Resources Journal*, 171, 104359. <https://doi.org/10.1016/j.advwatres.2022.104359>, 2023.
- 1110 Wang, J., Walter, B. A., Yao, F., Song, C., Ding, M., Maroof, A. S., Zhu, J., Fan, C., McAlister, J. M., Sikder, M. S., Sheng, Y., Allen, G. H., Crétaux, J.-F., and Wada, Y.: GeoDAR: georeferenced global dams and reservoirs database for bridging attributes and geolocations. *Earth System Science Data*, 14, 1869–1899. <https://doi.org/10.5194/essd-14-1869-2022>, 2022.
- 1115 Ward, A. S., Wondzell, S. M., Schmadel, N. M., and Herzog, S. P.: Climate Change Causes River Network Contraction and Disconnection in the H.J. Andrews Experimental Forest, Oregon, USA. *Frontiers in Water*, 2, 1–10. <https://doi.org/10.3389/frwa.2020.00007>, 2020.
- Werner, T. and Upper, C.: Time Variation in the Tail Behaviour of Bund Futures Returns, European Central Bank, Working Paper (199). <https://www.ecb.europa.eu/pub/pdf/scpwps/ecbwp199.pdf>, 2002.



- 1120 Wietzke, L. M., Merz, B., Gerlitz, L., Kreibich, H., Guse, B., Castellarin, A., and Vorogushyn, S.: Comparative analysis of scalar upper tail indicators. *Hydrological Sciences Journal*, 65(10), 1625–1639. <https://doi.org/10.1080/02626667.2020.1769104>, 2020.
- Wilcoxon, F.: Individual comparisons by ranking methods. *Biometrics Bulletin*, 1(6), 80–83. <https://doi.org/10.2307/3001968>, 1945.
- 1125 Wittenberg, H.: Baseflow recession and recharge as nonlinear storage processes. *Hydrological Processes*, 13(5), 715–726. [https://doi.org/10.1002/\(SICI\)1099-1085\(19990415\)13:5<715::AID-HYP775>3.0.CO;2-N](https://doi.org/10.1002/(SICI)1099-1085(19990415)13:5<715::AID-HYP775>3.0.CO;2-N), 1999.
- Wu, Q., Ke, L., Wang, J., Pavelsky, T. M., Allen, G. H., Sheng, Y., Duan, X., Zhu, Y., Wu, J., Wang, L., Liu, K., Chen, T., Zhang, W., Fan, C., Yong, B., and Song, C.: Satellites reveal hotspots of global river extent change. *Nature Communications*, 14(1). <https://doi.org/10.1038/s41467-023-37061-3>, 2023. EZomer, R. J., Xu, J., and Trabucco, A.: Version 3 of the Global Aridity Index and Potential Evapotranspiration Database. *Scientific Data*, 9(1), 1–15. [data set]. <https://doi.org/10.1038/s41597-022-01493-1> (last access: 25 November, 2023), 2022.
- 1130